Supplemental Appendix

Cool cities: The value of urban trees*

Lu Han Stephan Heblich Christopher Timmins
Yanos Zylberberg

March 30, 2026

*Han: University of Wisconsin at Madison, lu.han@wisc.edu; Heblich: University of Toronto, NBER, CESifo, stephan.heblich@utoronto.ca; Timmins: University of Wisconsin at Madison, NBER, ctimmins@wisc.edu; Zylberberg: University of Bristol, CEPR, yanos.zylberberg@bristol.ac.uk.

Table of Contents

This online appendix (A) places our context and experiment within the wider context of urban forestry across North-American cities, (B) provides further details about the data, (C) discusses treatment heterogeneity and robustness checks, and (D) details additional empirical results about temperature, energy consumption, and pollution.

A Tree canopy and temperature across North-American cities **1**

A.1 A dataset of North-American cities 1

A.2 Evolution of temperature and forest cover over time 2

A.3 The Emerald Ash Borer infestation 4

B Data appendix **6**

B.1 Tree canopy and land cover 6

B.2 Ash trees and the dynamics of urban forestry over time 8

B.3 Property values, energy consumption, temperature, and pollution 13

B.4 Descriptive statistics 17

C The value of trees—complements **21**

C.1 The heterogeneous value of trees 21

C.2 Robustness checks 24

D Tree canopy, temperature, energy consumption, and pollution **28**

D.1 The cooling effect of urban forestry 28

D.2 Energy consumption 29

D.3 The quantitative role of energy savings 35

D.4 Tree canopy and pollution 37

References **41**

A Tree canopy and temperature across North-American cities

This section sheds light on the evolution of forest cover and temperature across North-American cities and describes our main experiment—the Emerald Ash Borer (EAB) infestation in Toronto—within this wider context.

Figure A1. The distribution of tree canopy and temperature across North-American cities.

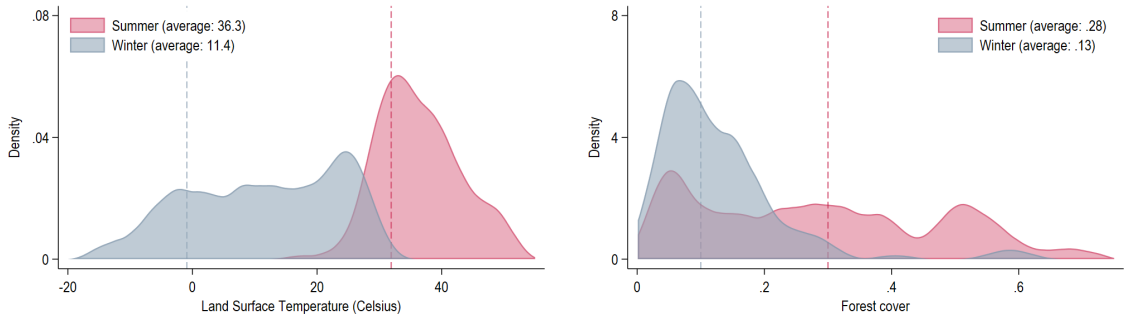

(a) Land Surface Temperature

(b) Forest cover

Notes: Panel (a) displays the distribution of Land Surface Temperature (Celsius degrees) in 2015 across 122 Canadian and American cities with more than 200,000 inhabitants (based on the procedure developed in Ermida et al., 2020). We distinguish the Winter season (in blue) from the Summer season (in red). Note that Land Surface Temperature usually differs from air temperature, and this difference can be higher than 10 Celsius degrees during Summer (Naserikia et al., 2023). Panel (b) displays the distribution of forest cover in 2015 across the same cities (again based on the procedure developed in Ermida et al., 2020). We display the sample average in the legend, and we show the Toronto average as a dashed line.

A.1 A dataset of North-American cities

In this section, the analysis relies on a cartographic dataset of American and Canadian cities compiled from Census boundary files around 2010.[1] We restrict the main analysis to cities with more than 200,000 inhabitants, leaving us with 122 agglomerations across Canada and the United States. We combine these geographies with data constructed from satellite imagery to construct averages at the city level over time: Land Surface Temperature in Celsius degrees, Normalized Difference Vegetation Index, forest cover using the Thermal Infrared (TIRS) band provided by Landsat L5 (1985–1999), Landsat L7 (1999–2013) and Landsat L8 (2013–2018) and the procedure developed in Ermida et al. (2020); monthly maximum/minimum temperatures and wind-speed at 10m using TerraClimate (Abatzoglou et al., 2018); typical monthly temperature and precipitation using WorldClim (Hijmans et al., 2005); land cover in recent period from ESA WorldCover 10m

[1] In Canada, we collect the census metropolitan areas and census agglomerations boundaries provided by the Boundary Files (2016 Census, Statistics Canada Catalogue no. 92-160-X) and restrict the sample to cities with more than 200,000 inhabitants. In the United States, we rely on the 500 Cities Project developed by the Centers for Disease Control and Prevention and based on the 2010 Census files.

(Zanaga et al., 2022) and Dynamic World 10m (Brown et al., 2022); topographic data (from the SRTM 90m Digital Elevation Data and the Global ALOS mTPI, see Jarvis et al., 2008; Theobald et al., 2015); and soil content/bulk (Hengl, 2018; Hengl and Wheeler, 2018).

Figure A1 shows the distribution of tree canopy and temperature across these cities during Winter and Summer. The main take-away message is that: (i) there is large variation in temperatures during Winter due to climatic variation, but Land Surface Temperatures are generally high during Summer;[2] (ii) there is large variation in (Summer) forest cover across North-American cities, illustrating disparities in population density, green infrastructure, and climate; and (iii) the city of Toronto is not an outlier.

Figure A2. The evolution of tree canopy and temperature across North-American cities.

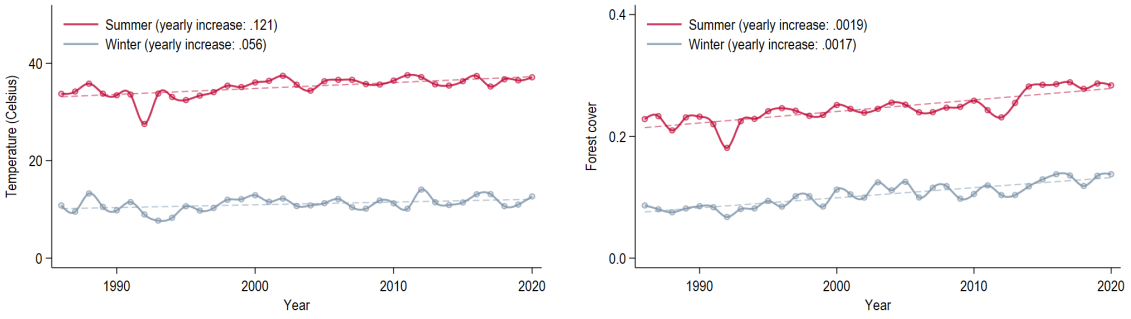

(a) Land Surface Temperature

(b) Forest cover

Notes: Panel (a) displays the average evolution of Land Surface Temperature in Celsius degrees from 1985 to 2020 (based on the procedure developed in Ermida et al., 2020). The blue line shows the average Land Surface Temperature during Winter (with the dashed line illustrating the best linear fit); and the red line shows the average Land Surface Temperature during Summer. Note that the Summer of 1992 was exceptionally cold in North America—one of the coldest Summer in a century. Panel (b) displays the average evolution of forest cover within the same sample of cities (Ermida et al., 2020). We report the yearly increases in tree canopy and temperature in the legend, e.g., the average Land Surface Temperature during Summer increases annually by 0.12 degrees (Celsius)—or by 4 degrees (Celsius) over the whole period. By contrast, the average Land Surface Temperature during Winter increases annually by 0.056 degrees (Celsius)—or by 2 degrees (Celsius) over the whole period.

A.2 Evolution of temperature and forest cover over time

Climate change, economic development, and public investment have affected temperature and forest cover in North-American cities. We illustrate these secular trends in Figure A2. First, Land Surface Temperature steadily increases between 1985 and 2020, especially during Summer: the surface of the average North-American city is 4 degrees (Celsius) warmer in 2020 than in 1985, due to changes in climate but also changes in pollutant concentration, in human activity, and in the nature of impervious areas. By contrast, the increase in Land Surface Temperature during the Winter season is around

[2]Land Surface Temperature might significantly differ from air temperature, as a function of seasons, the urban structure, and how the surface absorbs solar radiation (Naserikia et al., 2023).

2 degrees (Celsius). Second, this increase occurs in spite of an expansion of tree canopy: the average North-American city experiences an increase in the area share of forests of about 5-6 percentage points over the period (in spite of a stabilization/slight decrease in the 2010s, as documented in Nowak and Greenfield, 2018).

Figure A3. The correlation between tree canopy and temperature across North-American cities.

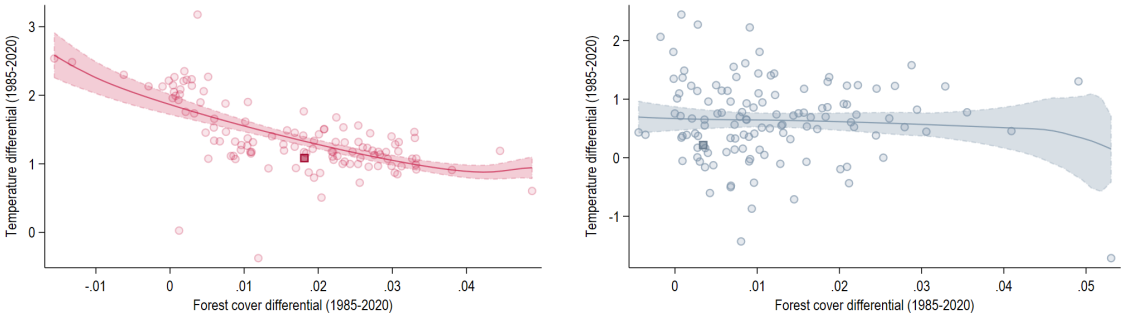

(a) Summer (b) Winter

Notes: Panel (a) displays the city-specific differential in Land Surface Temperature ($\overline{T}_{c,s}^{15-20} - \overline{T}_{c,s}^{85-90}$) as a function of the differential in forest cover ($\overline{\varphi}_{c,s}^{15-20} - \overline{\varphi}_{c,s}^{85-90}$), both computed during Summer, between 1985–1990 and 2015–2020. Panel (b) displays the city-specific differential in Land Surface Temperature ($\overline{T}_{c,w}^{15-20} - \overline{T}_{c,w}^{85-90}$) as a function of the differential in forest cover ($\overline{\varphi}_{c,w}^{15-20} - \overline{\varphi}_{c,w}^{85-90}$), both computed during Winter, between 1985–1990 and 2015–2020. In both panels, the city of Toronto is represented with a darker square. The lines are local polynomials of degree 1 with a bandwidth of 0.020; the 95% confidence interval is represented as the shaded area. The coefficients [standard errors] of a linear regression would be: -26.9 [3.1] in panel (a); and -6.2 [6.1] in panel (b).

Figure A2 however masks a large disparity in the dynamics of local temperature and forestry across different cities. In Figure A3, we display the city-specific differential in Land Surface Temperature and in forest cover from 1985–2020. More specifically, we correlate the Land Surface Temperature difference between 1985–1990 and 2015–2020 (y-axis) with the forest cover difference between 1985–1990 and 2015–2020 (x-axis)—during Summer (panel a) and Winter (panel b). We find a strong, negative correlation between local warming and forestry expansion: the gap in Summer temperature between the "most greening city" and the "least greening city" is around 1.5 degrees. A 0.01 relative loss in forest cover between 1985–1990 and 2015–2020 would be associated with an increase in Summer temperature of around 0.27 degrees (Celsius). Interestingly, this correlation—possibly indicative of the cooling effect of urban forestry—is not present for Winter temperatures (panel b): a 0.01 relative loss in forest cover would be associated with a very mild increase in Winter temperature of around 0.06 degrees (Celsius). How does the city of Toronto compare to other North-American cities? Toronto—highlighted with a square—becomes slightly greener than the average city and tends to experience a slightly lower increase in temperature. We will see next that it is the outcome of a secular greening of the city, in part mitigated by the EAB infestation.

Overall, the negative relationship between tree cover and temperature rise suggests

that urban forestry might help mitigate the impact of climate change and its interaction with the urban structure in a context where urban temperatures increase steadily and markedly so (Peng et al., 2012; Manoli et al., 2019). Our next section shows that the EAB infestation has offset part of the prior improvement in green infrastructure in Toronto over the past decades.

A.3 The Emerald Ash Borer infestation

Since 2002, the EAB infestation has spread across the North-East of the United States, from the most northern and eastern states to the south of West Virginia, Illinois, and Wisconsin, and throughout the bordering Canadian provinces of Ontario, Quebec, and Manitoba (Aukema et al., 2011; Herms and McCullough, 2014). The infestation has threatened a significant share of urban forestry, with Toronto being a prominent example. In theory, the loss of vulnerable ash trees would be sufficient to offset green investments over the past few decades (for example, the creation of parks or the development of green office buildings, as studied in Eichholtz et al., 2010).

Figure A4. The significant impact of the Emerald Ash Borer infestation in Toronto.

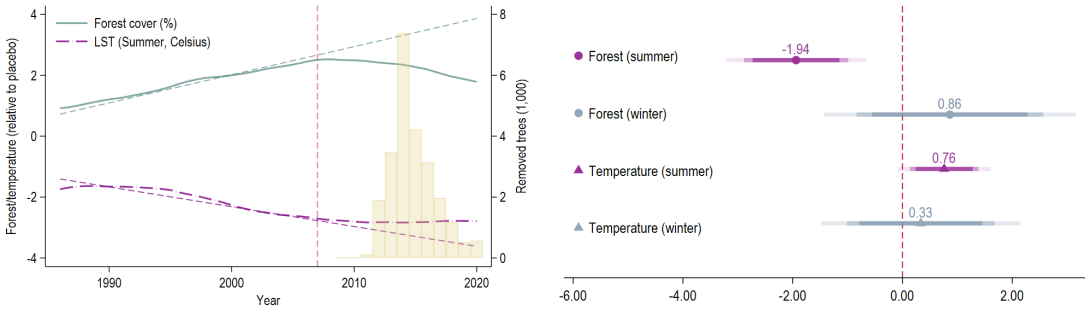

(a) An illustration

(b) Regression estimates

Notes: Panel (a) presents a local polynomial fit for the annual difference in forest cover (percentage points, green line) and average Land Surface Temperature during Summer months (Celsius degrees, purple line) between Toronto and a "placebo" group of *non-Northeastern* cities, defined as the 122 largest Canadian and American cities but the ones situated North and East compared to the most western and southern location of Illinois. The dashed lines show the best linear fit for these differences from 1985 to 2007. Additionally, the figure includes the yearly number of publicly-managed ash trees removed in Toronto (in thousands), based on a register of all tree-maintenance orders from the city's Parks and Forestry department (yellow bars). The vertical dashed line corresponds to the year 2007. Panel (b) displays the "average treatment effect" of the EAB infestation in Toronto, estimated using a stylized difference-in-differences specification where: (i) each observation is a city in a given year between 1985 and 2020; (ii) the time variation is a dummy equal to 1 if the year is post-2014; (iii) the cross-sectional variation (or treatment) is a dummy equal to 1 if the city is Toronto against a "placebo" group of cities (the *non-Northeastern* cities of our sample, where *Northeastern* cities are defined as all American and Canadian cities situated North and East compared to the most western and southern location of Illinois); (iv) the specification controls for (less localized) air temperature, precipitation, and wind speed (during the relevant season in a given year), city fixed effects and linear trends, differential trends along latitude, and year fixed effects; and (v) standard errors are clustered at the city level. The bands represent 10%, 5%, and 1% confidence intervals. For the sake of exposition, we consider forest cover in percentage points: Toronto lost 1.94 percentage points in Summer forest after 2014, relative to the placebo city; and Land Surface Temperature ended up being 0.76 Celsius degrees higher. Winter differentials are far less marked.

Figure A4 illustrates the aggregate impact of the EAB infestation on urban forestry

and its subsequent effect on local warming in the city of Toronto. The y-axis reports the average yearly difference in Land Surface Temperature (Celsius degrees) between Toronto and a "placebo" group of cities: the *non-Northeastern* cities of our sample.[3] Panel (a) shows that Toronto becomes cooler than the average placebo city, at least until 2007: from 2007 onward, the gap stabilizes or narrows down. Urban forestry provides a mirroring image: Toronto becomes greener than placebo cities until 2007, and from 2007 onward, the gap narrows down significantly. We benchmark these dynamics against the actual felling of ash trees, represented with yellow bars in the background of Figure A4 (a): the trend reversal in urban forestry seems to coincide with the timing of the EAB infestation. Had Toronto followed the pre-2007 trends in urban forestry and temperature between 2007–2020 as well, it would be 4 percentage points greener than the "placebo" group of cities (against 1.6 percentage points in reality) and 3.3-3.4 degrees cooler during Summer (against 2.8-2.9 degrees in reality).[4] Figure A4 (b) provides a more rigorous estimation of the previous differences between Toronto and "placebo" cities in a stylized difference-in-differences specification controlling for differential trends in latitude and climatic differences across cities. In line with the previous estimates, we find that: Toronto lost about 1.94 percentage points in Summer forest after 2014, relative to the placebo city; and Land Surface Temperature ended up being 0.76 Celsius degrees higher.

In summary, this Appendix section has shown that: (i) there has been a heterogeneous warming of North-American cities, in spite of a secular, long-run increase in urban forestry; (ii) cities investing most in urban trees have mitigated such warming; (iii) the city of Toronto was dealing with these secular trends better than the average; and (iv) the EAB infestation was sufficient in offsetting part of this positive trajectory.

[3] *Northeastern* cities are defined as all American and Canadian cities situated North and East compared to the most western and southern location of Illinois. Note that we could use a more convoluted approach based on synthetic difference-in-differences (Arkhangelsky et al., 2021), but each Northeastern city faces an infestation with different timing and intensity—implying that we would need to deal with a continuous, staggered treatment. Instead of using a placebo group of cities, we also constructed a synthetic control group comprising a weighted average of cities whose evolution of the tree canopy closely mirrors that of Toronto in the pre-infestation period (Abadie, 2021). Since the comparison between Toronto and other cities primarily serves as a motivational example and is not part of our main analysis, we opted for a simpler approach where we extrapolate the pre-trends. However, results from the synthetic control group exercise are available upon request.

[4] Under the assumption that the inflection in tree coverage is entirely attributable to the EAB infestation, our local and causal estimates of Section 4 would associate to this loss a 0.15-degree Celsius reduction in the average Land Surface Temperature. This is to be compared with a lower bound of 0.4 degrees between the actual temperature and its placebo level. The difference between the two estimates could indicate that our local identification of Section 4 ignores spillover effects across space and their interactions: the effect of trees on temperatures might go beyond the postal code and interact with the neighboring districts through heat trapping, air circulation, etc.—an interaction that is key to the formation of urban heat islands.

B Data appendix

This section complements Section 2 with: (i) a description of land cover and vegetation measures; (ii) an illustration of the dynamics of urban forestry over time using Google Street View and aerial data; (iii) a description of transactions across neighborhoods of Toronto; and (iv) additional details about the construction of the energy data. The publicly available data are published at Han et al. (2025).

B.1 Tree canopy and land cover

Land cover Our baseline specification relies on the land classification in 2007 and in 2018 provided by the Urban Forestry services of the City of Toronto and based upon high-resolution satellite imagery and LiDAR information (City of Toronto, 2019). The two exercises slightly differ in the availability of high-resolution satellite imagery, and no manual correction was performed in 2018, when some post-analysis manual corrections were performed in the pre-treatment land use classification. We illustrate the general variation in land cover across neighborhoods of Toronto in Figure 1 (a), distinguishing eight land classes: tree canopy; grass/shrub; bare earth; water; buildings; roads; other paved surfaces; and agriculture.

Vegetation indices from satellite imagery We complement and validate these measures of land cover with lower-resolution satellite imagery (Sentinel 2, 2016–2020, 10m resolution; Landsat L8, 2013–2020, 30m resolution; Landsat L7, 2007–2012, 30m resolution). One important benefit of using coarser, but more frequent, data is to shed light on the dynamics of tree cover over time (see Figure 2, panel b, in Section 2 for instance).

To construct vegetation, built-up and water indices, we proceed as follows for each collection of satellite imagery: (i) we isolate a summer period in any given year from June 1st to September 30th (to best capture vegetation); (ii) we construct a cloud-free mosaic of images taken during this period; (iii) we construct a set of indices, most notably, the Normalized Difference Vegetation Index (NDVI)—obtained by combining the reflection in the near-infrared spectrum (NIR) with the reflection in the red range of the spectrum (RED)—the Leaf Area Index (LAI), and the Normalized Difference Built-up Index (NDBI)—obtained by combining the reflection in the near-infrared spectrum (NIR) with the reflection in the short-wave infrared range of the spectrum (SWIR); and (iv) we construct the average indices within each postcode and every year covered by the collection. We illustrate the variation captured by NDVI and NDBI in Appendix Figure B1 (based on Sentinel S2 in 2018).

We use these indices to validate the land classification data and shed some light onto

Figure B1. Satellite imagery and vegetation/built-up indices (2018).

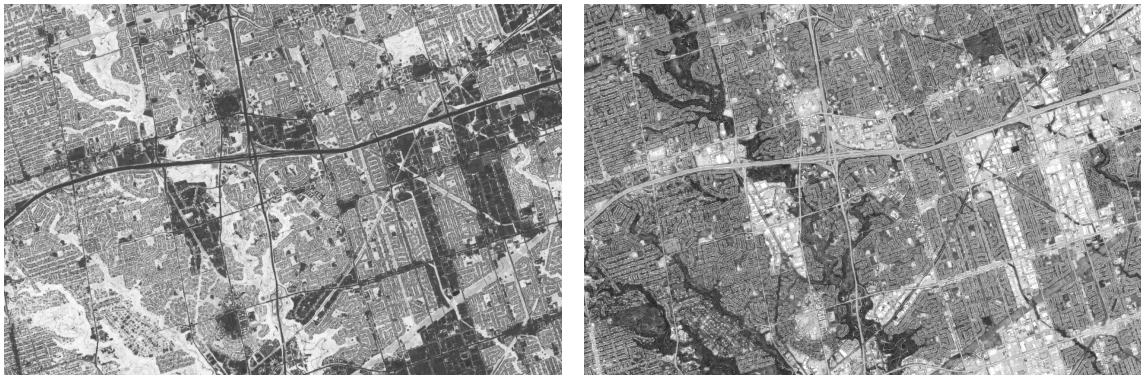

(a) NDVI (b) NDBI

Notes: This Figure displays vegetation against built-up indices, as constructed from a cloud-free mosaic of Sentinel imagery (S2, 10m resolution) covering May–September 2018 (North-East of Toronto). The Normalized Difference Vegetation Index (NDVI) is obtained by combining the reflection in the near-infrared spectrum (NIR) with the reflection in the red range of the spectrum (RED). The Normalized Difference Built-up Index (NDBI) is obtained by combining the reflection in the near-infrared spectrum (NIR) with the reflection in the short-wave infrared range of the spectrum (SWIR).

Figure B2. Validation of the measure of tree cover.

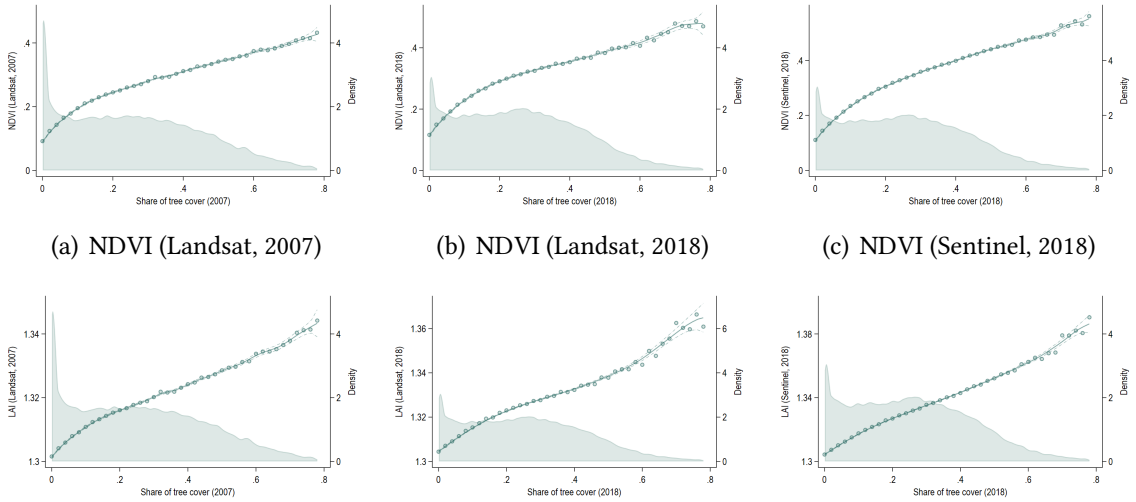

(a) NDVI (Landsat, 2007) (b) NDVI (Landsat, 2018) (c) NDVI (Sentinel, 2018)

(d) LAI (Landsat, 2007) (e) LAI (Landsat, 2018) (f) LAI (Sentinel, 2018)

Notes: This Figure correlates the measure of tree cover produced by Urban Forestry as part of an Urban Tree Canopy (UTC) Assessment in 2007 and 2018 with standard vegetation indices extracted from recent satellite imagery. Panels (a), (b) and (c) correlate the area share of tree canopy in 2007 and 2018 with the Normalized Difference Vegetation Index (NDVI) across postal codes. The NDVI is obtained by combining the reflection in the near-infrared spectrum (NIR) with the reflection in the red range of the spectrum (RED). Panels (d), (e) and (f) correlate the share of tree coverage in 2007 and 2018 with the Leaf Area Index (LAI) across postcodes. The green area displays the distribution of the x-axis variable for each panel. Panels (a) and (d) rely on a cloud-free mosaic of Landsat imagery (L7, 30m resolution) covering May–September 2007. Panels (b) and (e) rely on a cloud-free mosaic of Landsat imagery (L8, 30m resolution) covering May–September 2018. Panels (c) and (f) rely on a cloud-free mosaic of Sentinel imagery (S2, 10m resolution) covering May–September 2018.

the dynamics of urban forestry over our period of interest. In Figure B2, we correlate the measure of tree cover produced by Urban Forestry as part of an Urban Tree Canopy

(UTC) Assessment in 2007 and in 2018 with our vegetation indices, as extracted from recent satellite imagery (Landsat L7, Landsat L8, and Sentinel S2). We see that there is a very strong, positive, quasi-linear relationship between the area share covered by the tree canopy and the vegetation indices based on average reflectance across the visible, infra-red, near infra-red spectrum. These relationships are behind our findings of Section 2 where we show that a loss of 0.04-0.05 in the share of tree cover is accompanied by a decrease in the Normalized Difference Vegetation Index of 0.021 and in the Leaf Area Index of 0.0035. Figure B2 indeed shows that an additional 0.10 in tree cover corresponds to a 0.04 higher NDVI and a 0.005 higher LAI; a loss of 0.04-0.05 in tree canopy would thus be expected to decrease NDVI by 0.02 and LAI by 0.0025.

Figure B3. Removals and TreeAzin injections over time.

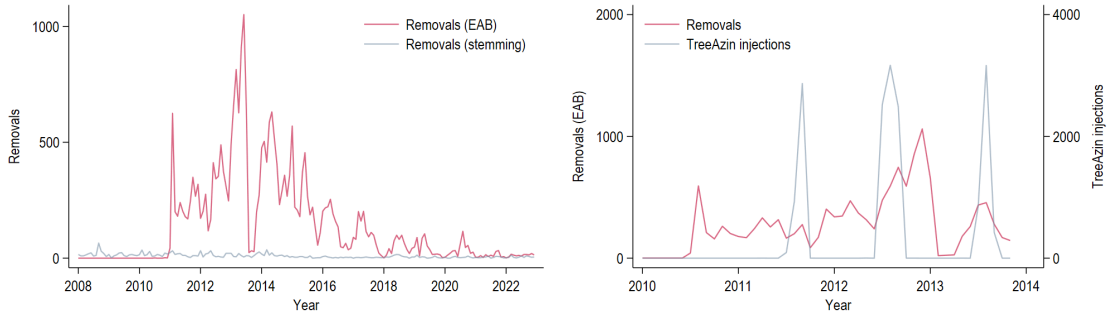

(a) Removals

(b) Injections

Notes: Panel (a) shows the evolution of tree removals between 2008 and 2023, distinguishing removals across the motive (EAB against stemming). Panel (b) shows the evolution of TreeAzin injections between 2010 and 2014 and compares it to the evolution of tree removals over the same period. The data source is the register of ash trees—a specific sub-module distinct from the general register of city-managed trees that we use in our baseline analysis (see Section 2 and Table 1 for instance).

B.2 Ash trees and the dynamics of urban forestry over time

The swift felling of ash trees and the distribution of injected trees In panel (b) of Figure 2 (Section 2), we show that most of the vegetation loss materializes between 2012–2016 in neighborhoods with high incidence of city-managed ash trees. We shed additional light on the swift felling of ash trees in Figure B3, where we exploit a specific dataset—distinct from the general register of city-managed trees—in which we do observe the planned and actual removals of city-managed ash trees between 2008 (and earlier) and 2023, and the injections of TreeAzin between 2012 and 2023 (both ordered by the City of Toronto). We find that removals steadily increase between 2010 and the autumn of 2013 (panel a), when the monthly incidence of removals reaches about 1,000 ash trees. It then gradually decreases until 2016–2017, in which less than 100 trees are removed each month. By contrast, TreeAzin injections are entirely concentrated in the

months of June, July and August every year (panel b)—when water and nutrients are most actively traveling upward through the bark.

Figure B4. Explaining TreeAzin injections.

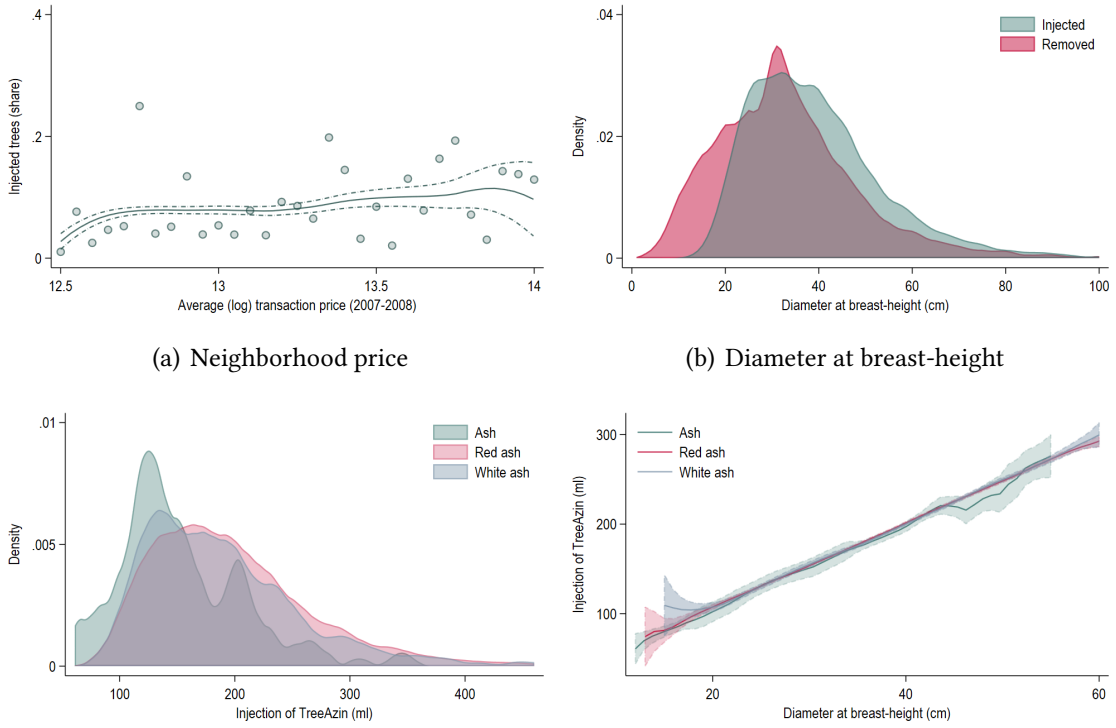

(a) Neighborhood price

(b) Diameter at breast-height

(c) Dosage across species

(d) Dosage across size

Notes: Panel (a) shows the correlation between the share of publicly-managed ash trees that are injected by TreeAzin from 2012 onward and the average (log) transaction price as recorded between 2007–2008 within a postal code. Panel (b) shows the distributions of diameters at breast-height for injected trees and removed trees. Panels (c) and (d) explain the dosage in milliliters (ml) for treated trees: (i) across tree species in panel (c); and (ii) as a function of tree size in panel (d).

Analyzing the decision to save or remove a tree is complicated: we have limited evidence nor insight about the decision process or the constraints hinging on the Parks and Forestry department of the City of Toronto.[5] Nonetheless, we do observe all TreeAzin injections, tree removals and other tree-maintenance orders from the Parks and Forestry department. In Figure B4, we correlate the share of injected trees among the publicly-managed ash trees within a postcode with housing prices at baseline (panel a), we show that injected trees tend to be slightly larger than removed trees, and we show that the dosage for treated trees is entirely explained by their size—the City of Toronto most likely provided a rule to the (external) contractors. We further "quantify" the role of tree characteristics, the way they are planted, and their neighborhood in a variance-

[5]For a more detailed discussion of ways to effectively protect urban ash trees, we refer interested readers to Sadof et al. (2023).

decomposition exercise where we regress removals/injections on: dummies for the exact tree species (e.g., red ash) and deciles of trunk diameters; dummies for the way they are planted (e.g, with pavers around the tree or as a container tree); and dummies for their ward. We find that tree characteristics explain 13% of the variance in whether the tree will be injected or removed; adding the planting structure explains 18%; and adding neighborhood fixed-effects explains 33%. In summary, geography and the age/species of the tree are the main predictors as to whether the tree will be saved or removed.

Figure B5. The dynamics of urban forestry over time—an illustration using the land use classification.



(a) Land cover (2007) (b) Land cover (2018)

Notes: Panels (a) and (b) show the land use classification in James Park Square (Scarborough, North-East of Toronto). The data was produced in 2007 and 2018 by Urban Forestry as part of an Urban Tree Canopy (UTC) Assessment, and land cover is represented by the following classes: tree canopy (dark green), grass/shrub (lighter green), bare earth (sand), water (dark blue), buildings (red), roads (dark gray), other paved surfaces (light gray) and agriculture (yellow). The green symbols represent the location of city-managed ash trees *at baseline*, as geolocated from their street addresses (Street Tree General Data, 2010).

A visual illustration In Section 2 and Figure 2 (b), we shed some light onto the swift decrease in vegetation cover experienced by neighborhoods with a high density of city-managed ash trees. Figure B5 (a/b) illustrates this systematic removal of infested ash trees, using James Park Square in Scarborough as an example, where baseline ash tree density was relatively high. We observe a significant reduction in tree canopy, represented in darker green. The loss in forest cover appears to correlate with the location of city-managed ash trees (green symbols), as geolocated in 2010, before the city proceeded to possible tree felling.

We provide a further illustration of the actual process of removal and replacement of city-managed trees in Figure B6. More specifically, we focus on the previous neighborhood depicted in Figure B5, James Park Square in Scarborough (North-East of Toronto), which experienced a massive loss in tree cover between 2007 and 2018 due to its rows of city-managed ash trees. Figure B6 presents successive street views of this neighborhood in 2007, 2014, and 2020. We see that the neighborhood is a typical leafy suburb in

Figure B6. The dynamics of urban forestry over time—an illustration using Google Street View.

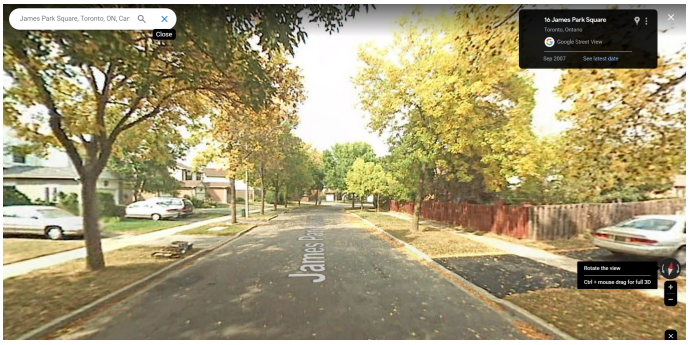

(a) 2007



(b) 2014



(c) 2020

Notes: This Figure shows three snapshots of the neighborhood depicted in Figure B5 (James Park Square, Scarborough, North-East of Toronto)—with a relatively high density of ash trees at baseline. The images were extracted in 2007 (panel a, before the infestation), 2014 (panel b, after the cut-downs), and 2020 (panel c, with replanted tree saplings) from Google Maps.

2007, with individual homes, private gardens, and rows of city-managed (ash) trees. In 2014, the mature ash trees are already cut down and replaced by young sprouts, leading to a significant change in the visual appeal of the neighborhood and in shade coverage. In 2020, the substitute sprouts have grown into tree saplings, still short of providing any significant tree cover, shade or sheltering against wind. As argued in Section 2, the felling of mature trees induces a loss in tree canopy that cannot be mitigated within a span of 25-30 years.

Figure B7. Transactions and low-income households across the City of Toronto.

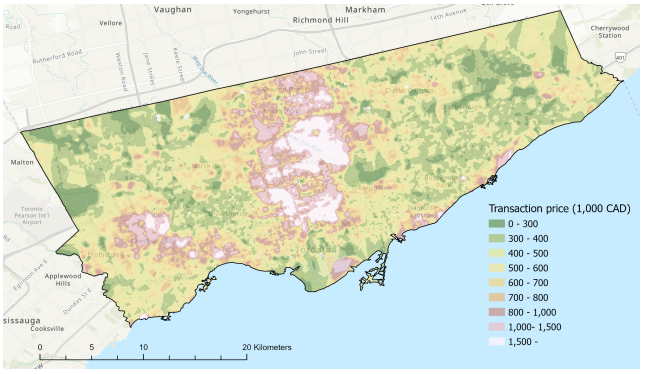

(a) Transaction price

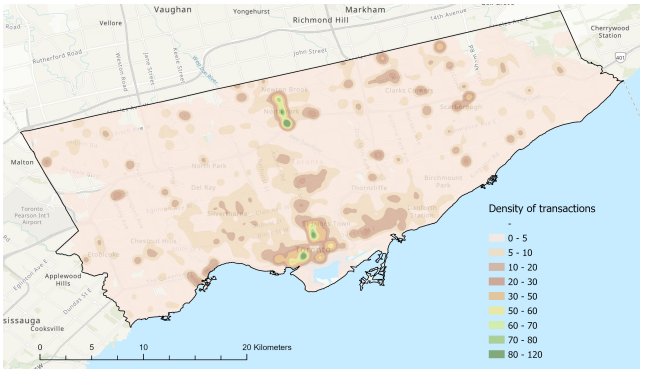

(b) Number of transactions

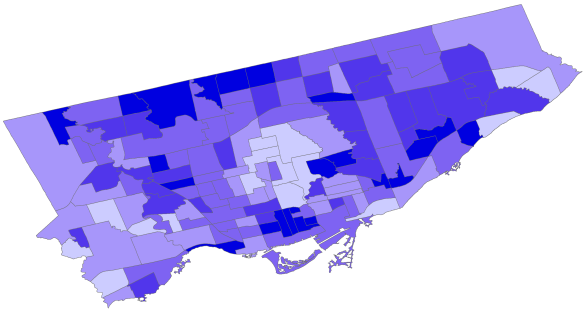

(c) Low-income

Notes: Panel (a) shows the average transaction price for all transactions between 2007 and 2020 in 1,000 CAD (from green to yellow to pink and then white, as standard in an elevation scale). One can see that the stretch between Yorkville and North York, Chestnut Hills (West of Toronto), and a few coastal neighborhoods are the neighborhoods with the highest transaction prices. Panel (b) displays the geography of property transactions between 2007 and 2020 across the City of Toronto. Each color class represents a bin of density (from white to pink to yellow and then green, as an inverted elevation scale). Note that the density is obtained through a kernel density procedure such that the scale does not have an easily-interpretable unit. Panel (c) displays the 2011 share of low-income households at the Forward Sortation Area (FSA, about 140 of them cover the City of Toronto), consisting of the first three characters of a postal code (e.g., "M5S" when a postal code is "M5S 1A1"). In the latter figure, color cut-offs are at 10%, 15%, 20%, and 25% from white to darker blue.

B.3 Property values, energy consumption, temperature, and pollution

The geography of property transactions and income The transaction data used in Section 4 and described in Section 2 cover the whole City of Toronto from 2007 to 2020. Note that we also have transaction data from 2002 to 2006—used in a robustness check—, but without detailed dwelling characteristics (see panel A of Table C3).[6]

In this Appendix, we illustrate the geography of the housing market in Figure B7, where we display the average transaction price in panel (a), the density of transactions in panel (b), and a measure of deprivation in panel (c). One can see that a few neighborhoods are highly demanded, most notably the area between Bloor-Yorkville and North York. This area is quite green, traversed by ravines, as shown in Figure 1 (a) of the paper. The correlation between transaction prices and the density of city-managed ash trees is however unclear at the neighborhood level (see Table B2 for a more systematic exploration of this correlation): the neighborhoods of Mount Pleasant, North York, Scarborough (East), and Etobicoke are the ones with the highest density of ash trees, but while the former two are quite demanded, Etobicoke is less demanded and Scarborough is considered a relatively deprived area (compared to the rest of the City of Toronto).

Figure B8. The cooling effect of urban forestry—an illustration during the heatwave in 2018.



(a) NDVI (b) Land Surface Temperature

Notes: This Figure exploits Landsat 8 satellite imagery in July and August 2018. The left panel shows the Normalized Difference Vegetation Index (NDVI) where green colors indicate a higher vegetation cover. The right panel shows the Land Surface Temperature (LST) where red colors indicate higher temperatures.

[6]We complement the transaction data with neighborhood characteristics from the register of the City of Toronto that includes detailed information about green spaces, protected ravines, property boundaries, building footprints, the general urban infrastructure, and school locations. We employ this cartographic information to calculate distance to amenities and other controls capturing neighborhood quality.

Tree canopy and temperature In the paper, we estimate the cooling effect of the tree canopy during heatwaves. Figure B8 further illustrates the correlation between urban temperature and urban forestry. We construct an average mosaic of Landsat 8 satellite imagery in July and August 2018 and consider two indices based on the relative reflectance of different bands: the Normalized Difference Vegetation Index (NDVI) capturing vegetation cover; and the Land Surface Temperature (LST) which we also calculate at a 30-meter spatial resolution.[7] The left panel of Figure B8 displays the average Normalized Difference Vegetation Index over the period, and the right panel shows the average Land Surface Temperature across two adjacent neighborhoods with significant differences in tree canopy coverage (South Parkdale, South-West of Toronto). We observe a sharp difference between the West and the East of Dufferin St: the tree coverage in the West of Dufferin St markedly alleviates the rise in temperature during this heat wave episode.

Figure B9. The cooling effect of urban forestry—a map of Toronto during the heatwave in 2018.

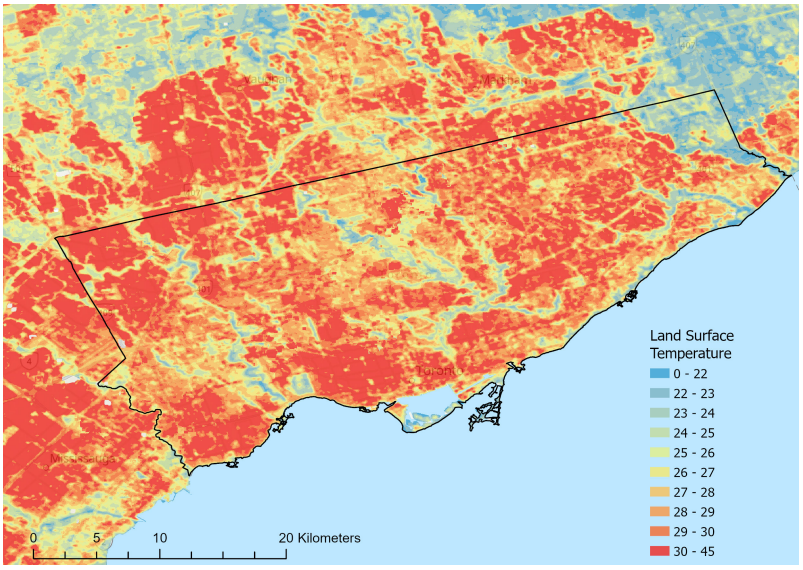

Notes: This Figure displays the average Land Surface Temperature (LST in Celsius degrees) across the City of Toronto during July and August 2018. Blue to red colors indicate higher temperatures.

We shed additional light on the urban heat island effect and the role of urban forestry in Figure B9, where we display the Land Surface Temperature (LST) for the months of July and August 2018 across the City of Toronto and its immediate hinterlands. There are two salient observations. First, there is a very significant temperature differential (of the

[7]The two measures share some small, mechanical correlation because the LST calculations employ a fractional vegetation measure that is based on the ratio of the maximum and minimum values of the NDVI to correct the temperature measure derived from the Thermal Infrared (TIRS) band (see Ermida et al., 2020; Li et al., 2023, for more details).

order of magnitude of 5 degrees) between the city and its hinterlands. This is within the interval of urban island effects estimated in Manoli et al. (2019) across many cities of the developed and developing World. Second, there is some variation within neighborhoods of the City of Toronto: for instance, one can distinctly see the temperature gradient between the numerous ravines, forming a large ravine system and hosting a dense urban forest, and the impervious areas surrounding those ravines.

Energy consumption We secured access to detailed energy consumption data. For the period 2011–2015, we observe households' energy consumption per billing period which allows us to estimate weekly energy consumption; for the period 2011–2021, we observe the average energy consumption per month and postcode. We will now describe these two datasets in more detail.

In the raw data for the period 2011–2015, energy consumption is reported in kilowatt hours (kWh) adjusted for line losses over the billing period. The days of service in a billing period range between 1 and 2 months and we know the start and end date of each billing period which varies across households. To calculate energy consumption in postcode p, week w and year t, we construct a daily panel of each household i's average daily energy consumption and estimate:

$$e_{ipwt} = \alpha_i + E_{pwt} + \epsilon_{ipwt}$$

where the fixed effects E_{pwt} capture the average daily energy consumption in postcode p for a given week w of year t. To derive a measure e_{pwt} of the average energy consumption per week and year, we multiply the average daily energy consumption e_{ipwt} by seven (days per week). One nice feature of our electricity data is that we can condition the estimation on energy meter fixed effects, α_i, which absorb all time-invariant house and occupant characteristics. The latter characteristics control, for example, for the energy efficiency of the house. We will use this shorter, weekly panel in a robustness check that exploits the shading potential of trees (see Appendix D.2).

In addition to the weekly data, we have access to the average energy and gas consumption for every Toronto postcode (censored below a minimum of five households) in a monthly panel spanning from 2011 to 2019 (gas) and 2022 (electricity). There are important seasonal patterns in energy consumption which we illustrate in Figure B10. Electricity consumption is high in the summer months, due to the use of air conditioning. Between November–April, electricity consumption is a mix of light and electrical heating, even though natural gas is the most common source of heating fuel. Consequently, we would expect trees to have more pronounced electricity consumption effects in the summer. Natural gas is used for heating during these winter months and there is indeed

Figure B10. Electricity and gas consumption over time.

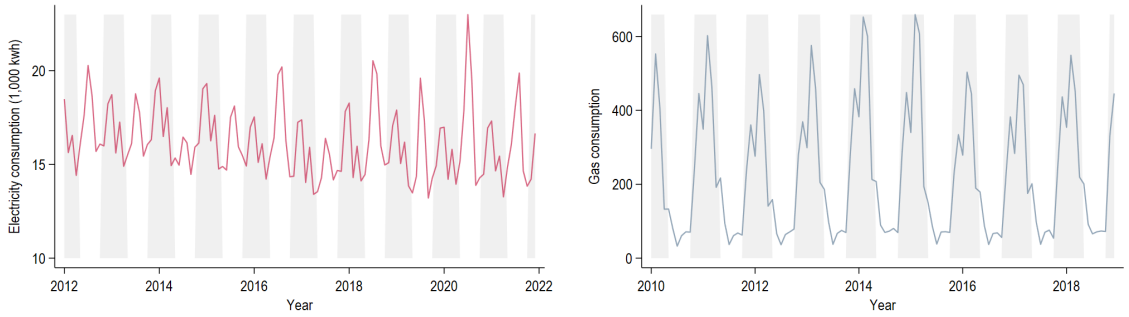

(a) Electricity (b) Natural gas

Notes: The left panel of the graph shows the adjusted monthly electricity consumption measured in kWh across postcodes in Toronto. The right panel shows the average monthly consumption of natural gas measured in cubic meters across postcodes in Toronto. Gray shaded areas indicate winter months, i.e., November–April.

a significantly higher usage of natural gas in these months with a spike in January and February, the coldest months. We use both measures to estimate the effects of urban forestry on energy consumption (Table 2 of the paper and Appendix D.2).

Figure B11. PM2.5 concentration in July 2007.

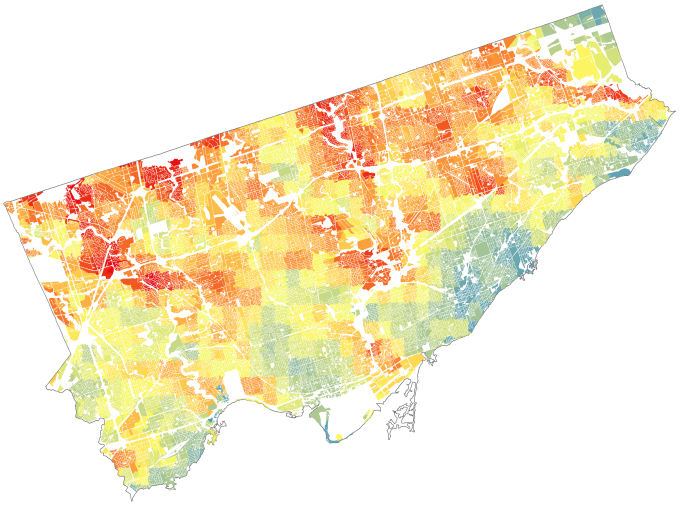

Notes: This Figure displays the PM2.5 concentration as recorded in July 2007 and nested at the level of postal codes. The color scale goes from light blue to red (corresponding to equal intervals of pollution between 9 $\mu g/m^3$ to 13 $\mu g/m^3$). The data is based on Aerosol Optical Depth (AOD) measures from NASA MODIS (250m horizontal resolution), NASA MISR (about 1.1 km horizontal resolution), and NASA SeaWIFS (to cover the oceans). Source: Van Donkelaar et al. (2021), and CANUE.

Pollution We rely on monthly estimates of fine particulate matter (PM2.5) provided by Van Donkelaar et al. (2021) for the period 1998–2021.[8] The data is based on Aerosol Optical Depth (AOD) measures from NASA MODIS (250m horizontal resolution), NASA MISR (about 1.1 km horizontal resolution), and NASA SeaWIFS (to cover the oceans). These satellite-based measures are combined with a dispersion model (i.e., the GEOS-Chem chemical transport model, see Van Donkelaar et al., 2021), which is calibrated using a subsample of ground-based observations.

A main input (and significant constraint on spatial resolution) is the Aerosol Optical Depth (AOD) from MODIS, inducing a coarser spatial resolution than in our other satellite-based measures (and further justifying a clustering at a higher geographic level—ward in our baseline specification). We illustrate the resulting variation in fine particulate matter nested across postal codes in Figure B11, where we display PM2.5 concentration in July 2007. One can see that there is still significant local variation, partly explained by the location of the main entry/exit points to/from the city—the Don Valley Parkway in the center of the map, Toronto Pearson airport (West), or the King's Highway 401. One corollary is that there might exist a spurious correlation between urban forestry (e.g., along the Don Valley) and air pollution. Our empirical strategy arguably addresses this issue.

B.4 Descriptive statistics

This Appendix provides some descriptive statistics that aim to provide a better understanding of the variation underlying the identification strategy.

Urban forestry We start by reporting descriptive statistics about transaction data in Table B1: the mean and standard deviations of the main variables, control variables and their values for transactions in postal codes with above- or below-median tree canopy. As apparent in Table B1, there are wide differences in tree density across postal codes. Postcodes with above-median tree density have about five times more tree cover than postcodes with below-median tree density in 2007. Local urban forestry correlates with property prices, which are about 35% higher for properties with above-median tree density. This price differential may illustrate a tree premium, but they also seem to indicate differential property characteristics—properties with above-median tree density have, on average, 0.7 additional bedrooms and 1.1 additional rooms—and neighborhood quality in general—postal codes with above-median tree density are higher income neighborhoods.

[8]The data is available on the CANUE website. Acknowledgments: PM2.5 metrics, indexed to DMTI Spatial Inc. postal codes, were provided by CANUE (Canadian Urban Environmental Health Research Consortium).

Table B1. Descriptive statistics.

			Tree density	
	Mean	*Stand. dev.*	High	Low
Panel A: Transaction characteristics				
Transaction price (log)	13.14	*0.655*	13.31	12.97
Number of bedrooms	2.108	*1.333*	2.442	1.774
Number of rooms	4.975	*2.851*	5.521	4.428
Panel B: Neighborhood characteristics				
Low-income households	18.64	*6.404*	17.61	19.67
Distance to school (m)	395.4	*246.6*	362.6	428.2
Panel C: Land cover in 2007				
Tree canopy	0.234	*0.189*	0.390	0.077
Grass/shrub	0.158	*0.120*	0.179	0.138
Bare earth	0.005	*0.060*	0.001	0.010
Water	0.001	*0.008*	0.001	0.001
Buildings	0.228	*0.154*	0.190	0.265
Roads	0.159	*0.162*	0.113	0.205
Other paved surfaces	0.215	*0.200*	0.126	0.305
Agriculture	0.000	*0.002*	0.000	0.000
Panel D: City-managed trees				
Ash trees (density, per sq. km)	81.15	*266.8*	88.23	74.07
All trees (density, per sq. km)	1964	*2034*	2180	1748
Observations	440,798		220,399	220,399

Notes: All statistics are computed using the baseline sample of transactions; standard deviations are reported in *italics*. The samples of high- and low-tree density are defined with respect to the median share of tree canopy as produced by Urban Forestry as part of the Urban Tree Canopy Assessment in 2007 (first row of *Panel C: Land cover in 2007*). The share of low-income households is computed in 2011 and provided at the Forward Sortation Area (FSA, about 140 of them cover the City of Toronto), consisting of the first three characters of a postal code (e.g., "M5S" when a postal code is "M5S 1A1").

Panels (a) and (b) of Figure B12 show the correlation between house prices and the surrounding urban forestry. The x-axis is the area share of tree cover in 2007, TD_{p2007}; and the y-axis is the average (log) house price. The association between transaction prices and tree density should reflect the price premium associated with leafy suburbs, but also the opportunity cost of maintaining urban forestry. As shown in panel (a), this correlation is positive for almost any share of tree cover in 2007, especially so in residential areas with significant urban forestry. Panel (b) displays the same relationship conditioning on our main control variables: the number of bedrooms and rooms; latitude, longitude; and ward fixed effects—all interacted with year fixed effects. As apparent, the price gradient between less and more leafy neighborhoods remains substantial. Panels (c) and (d) show a strongly negative correlation between summer temperatures (June-September 2018), T_p, and the surrounding urban forestry. There is an average difference of about four degrees Celsius between postcodes with very low versus very high tree cover. This holds true even when conditioning on ward fixed effects and our

Figure B12. Housing prices, temperature, and density of the tree canopy.

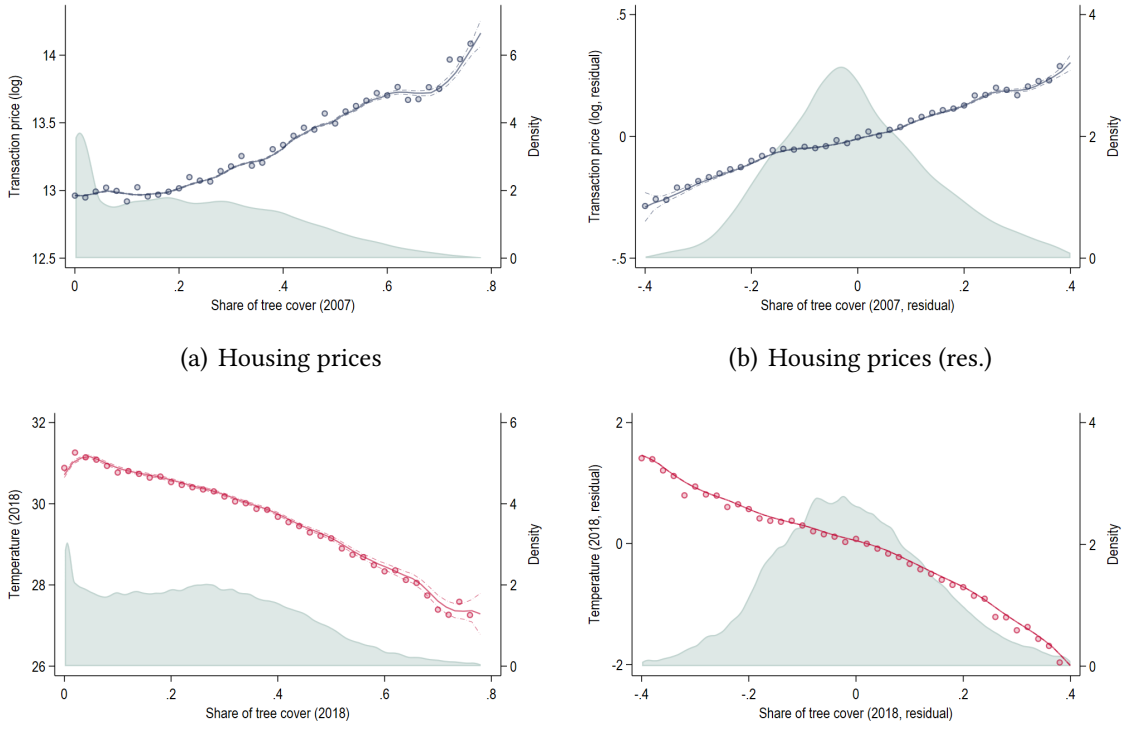

(a) Housing prices

(b) Housing prices (res.)

(c) Temperature

(d) Temperature (res.)

Notes: Panel (a) represents the relationship between the (logarithm) transaction price and our measure of tree cover at the postcode level. We group transactions by bins of tree cover: the dots represent the average transaction price within each bin. The green area represents the distribution of the x-axis variable across all panels. Panel (b) represents the same relationship in which the (logarithm) transaction price and the tree cover within the postcode are residualized: we regress both measures on the number of bedrooms, the number of rooms, the latitude, the longitude, ward fixed effects—all interacted with year fixed effects. Panel (c) represents the relationship between the average temperature during the summer in 2018 and our measure of tree cover at the postcode level (with a buffer of 10m around the postcode shape and in 2018). We group postal codes by bins of tree cover: the dots represent the average temperature within each bin. Panel (d) represents the same relationship in which the temperature and the tree cover within the postcode are residualized: we regress both measures on the latitude, the longitude, and ward fixed effects. The lines are locally weighted regression on all observations.

baseline controls.

Distribution of city-managed ash trees Finally, our empirical strategy relies on the initial distribution of city-managed ash trees across postal codes (and within wards). While urban forestry is very predictive of neighborhood characteristics, the allocation of publicly-maintained *ash* trees is less informative of neighborhood quality. We shed some light onto this relationship in Table B2 where we report transaction characteristics (Panel A), neighborhood characteristics (Panel B), initial land cover (Panel C), and the allocation of publicly-maintained trees (Panel D) for four types of neighborhoods: (i) postal codes without any city-managed ash trees (Q1) and (ii) tertiles of city-managed ash tree density for postal codes with at least one city-managed ash tree (Q2, Q3, Q4).

Table B2. Descriptive statistics and the spatial distribution of ash trees.

Quartiles of ash tree density	Q1	Q2	Q3	Q4
Panel A: Transaction characteristics				
Transaction price (log)	13.13	13.35	13.18	13.10
Number of bedrooms	2.031	2.624	2.364	2.357
Number of rooms	4.857	5.806	5.366	5.309
Panel B: Neighborhood characteristics				
Low-income households	18.79	18.05	18.04	17.79
Distance to school (m)	407.7	295.5	341.3	387.0
Panel C: Land cover in 2007				
Tree canopy	0.221	0.334	0.283	0.243
Grass/shrub	0.151	0.204	0.182	0.184
Bare earth	0.006	0.002	0.002	0.003
Water	0.001	0.002	0.000	0.002
Buildings	0.230	0.201	0.228	0.220
Roads	0.162	0.126	0.145	0.166
Other paved surfaces	0.228	0.131	0.160	0.182
Agriculture	0.000	0.000	0.000	0.000
Panel D: City-managed trees				
Ash trees (density, per sq. km)	0	87.09	252.3	988.4
All trees (density, per sq. km)	1908	1889	2029	2728
Observations	359,428	27,124	27,452	26,794

Notes: All statistics are computed using the baseline sample—a unit is a transaction. Q1 represents the sample of transactions with 0 ash trees within 10 meters of the postal code. Q2, Q3, and Q4 represents tertiles in terms of ash tree density (see the first row of *Panel D: City-managed trees*) among transactions for which there is at least one ash tree within 10 meters of the postal code. The share of low-income households is computed in 2011 and provided at the Forward Sortation Area (FSA, about 140 of them cover the City of Toronto), consisting of the first three characters of a postal code (e.g., "M5S" when a postal code is "M5S 1A1").

Postal codes without any publicly-maintained ash tree appear to be negatively selected, but the relationship between neighborhood quality and ash tree density is far less clear across postal codes with some city-managed ash trees

C The value of trees—complements

C.1 The heterogeneous value of trees

This section sheds some light onto the unequal distribution of urban forestry and the possibly heterogeneous value of urban trees.

Figure C1. Deprivation and density of the tree canopy.

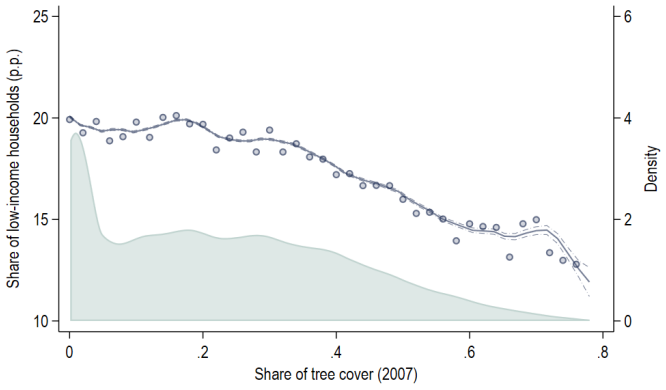

Notes: This Figure represents the relationship between the share of low-income households at the Forward Sortation Area level (first three characters of a postal code)—but nested within postal codes—and our measure of tree cover at the postcode level. We group transactions by bins of tree cover: the dots represent the average share of low-income households within each bin. The green area represents the distribution of the x-axis variable across all panels. The lines are locally weighted regression on all observations.

The unequal distribution of urban forestry The distribution of urban forestry is unequal across space, as documented in Section B.4. The prevalence of trees interacts with neighborhood characteristics in a systematic manner. We illustrate the inequalities in access to urban trees in Figure C1 where we correlate the density of the local tree canopy with a deprivation measure, i.e., the share of low-income households. We find that the average share of low-income households is around 20% in neighborhoods without any tree versus 12% in the leafiest postal codes.

The heterogeneous value of (the marginal) trees The unequal distribution of urban forestry could illustrate the heterogeneous value of (the marginal) trees: trees might be highly valued in richer, less densely-populated neighborhoods with larger properties. In such a context, they might have higher aesthetic value (Benson et al., 1998; Price, 2003; Todorova et al., 2004) and better complement the "consumption of the public space" by residents. We evaluate the heterogeneous treatment effects of trees on transaction prices in Table C1 where we interact our treatment with a measure of deprivation (a dummy equal to 1 if the share of low-income households is above median when nested at the level of a postal code), a measure of public provision of green areas (a dummy equal to

Table C1. The amenity value of trees—heterogeneous treatment effects.

Transaction price (log)	(1)	(2)	(3)	(4)
Tree cover	1.267	1.417	0.786	1.117
	(0.487)	(0.574)	(0.386)	(0.673)
Tree cover × Deprived	-0.643			
	(0.573)			
Tree cover × Distance to green		-0.632		
		(0.390)		
Tree cover × Tree density			0.362	
			(0.152)	
Tree cover × Tree density (Q1)				-2.303
				(3.172)
Tree cover × Tree density (Q2)				0.921
				(5.975)
Tree cover × Tree density (Q3)				0.043
				(1.025)
Observations	15,884	15,884	15,884	15,884
F-statistic 1	14.40	19.15	21.04	26.89
F-statistic 2	7.77	12.58	14.48	3.56
F-statistic 3	-	-	-	0.92
F-statistic 4	-	-	-	19.52

Notes: Standard errors are reported between parentheses and are clustered at the ward level. The dependent variable is the average (log) transaction price during the post-period. All columns report the estimates from an IV specification in which the unit of observation is a postal code and the tree cover in 2018 (and its interaction) is instrumented by the baseline density of city-managed ash trees (and its interaction). All specifications include: the average (log) transaction price during the pre-period; the interacted variable; ward fixed effects; a measure of city-managed tree density; latitude and longitude; area shares from the land classification in 2007 (tree canopy, grass/shrub, bare earth, water, buildings, roads, other paved surfaces and agriculture); transaction controls in the pre-period and in the post-period, including the number of rooms, the number of bedrooms, and 10 dwelling types (e.g., detached, apartment, duplex, commercial). *Deprived* is a dummy equal to 1 if the share of low-income households is above median within a postal code—the share of low-income households is computed in 2011, provided at the Forward Sortation Area (consisting of the first three characters of a postal code, e.g., "M5S" when a postal code is "M5S 1A1"), and then nested at the postal code level. *Distance to green* is a dummy equal to 1 if the distance to green areas is within the last three quartiles (across postal codes) in 2007. *Tree density* is a standardized measure of (private and public) tree density within 50 meters of the postal code in 2007. *Tree density (Q1/2/3)* are the first, second, and third quantiles of (private and public) tree density within 50 meters of the postal code in 2007. F-statistics are derived using the weak instrument F-test proposed in Sanderson and Windmeijer (2016).

the distance to green areas is within the last three quartiles across postal codes in 2007), and a measure of greenness—the standardized density of (private and public) trees within 50 meters of the postal code. While this specification is demanding and statistical power is limited, we find some supportive evidence that the treatment effect is larger in richer areas: one additional percentage point in tree cover within a postcode increases property

prices by 1.27% in less deprived neighborhoods versus 0.63% in deprived neighborhoods (column 1). The treatment effect tends to be larger in postal codes with easier access to green areas (e.g., parks, column 2) and in postal codes that were originally quite green (column 3, replicating column 1 of Table 2, Panel B in the paper). About the latter effect, a standard deviation in initial tree density in 2007 increases the treatment effect by about 0.36, from an average treatment effect of 1.13. In column (4), we construct bins in order to shed light on the shape of non-linearities in treatment effect, but the specification becomes unfortunately under-powered.

Table C2. The heterogeneous value of trees—robustness checks.

Transaction price (log)	(1)	(2)
Tree cover	1.240	1.258
	(0.468)	(0.575)
Tree cover × Tree density	0.293	0.330
	(0.173)	(0.143)
Observations	15,884	15,884
F-statistic 1	14.99	17.82
F-statistic 2	13.23	14.02
F-statistic 3	7.76	12.80

Notes: Standard errors are reported between parentheses and are clustered at the ward level. This table reports the estimates from an IV specification in which the unit of observation is a postal code and the tree cover in 2018 (and its interaction) is instrumented by the baseline density of city-managed ash trees (and its interaction), controlling for the baseline density of city-managed ash trees interacted with confounders: a dummy equal to 1 if the share of low-income households is above median within a postal code in column (1); and a dummy equal to 1 if the distance to green areas is within the last three quartiles (across postal codes) in 2007 in column (2). Note that the share of low-income households is computed in 2011, provided at the Forward Sortation Area (consisting of the first three characters of a postal code, e.g., "M5S" when a postal code is "M5S 1A1"), and then nested at the postal code level. All specifications condition on the interacted variables, *Tree density* and the confounders. *Tree density* is a standardized measure of (private and public) tree density within 50 meters of the postal code in 2007. In these specifications with three instruments and three endogenous variables, F-statistics are derived using the weak instrument F-test proposed in Sanderson and Windmeijer (2016).

One concern with the previous analysis and our headline heterogeneity exploration in Table 2 (Panel B) is that the non-linear hedonic valuation of urban forestry could reflect confounders that are correlated with baseline tree density (e.g., neighborhood quality, see Figure C1). In Table C2, we thus replicate the exercise of column (1) of Table 2 (Panel B), reproduced in column (3) of Table C1, adding the interaction of the endogenous variable with: a dummy equal to 1 if the share of low-income households is above median within a postal code in column (1); and a dummy equal to 1 if the distance to green areas is within the last three quartiles (across postal codes) in 2007 in column (2). In these specifications with three instruments and three endogenous variables, the marginal premium in tree valuation associated with one standard deviation in baseline tree density remains quite stable (0.29 and 0.33, versus 0.36 in column 3 of Table C1).

Table C3. The amenity value of trees—robustness checks.

Transaction price (log)	(1)	(2)	(3)
Panel A: Placebo specification (2002–2006)			
Tree cover	0.327	0.070	0.118
	(0.284)	(0.232)	(0.283)
Cut-off	2003–2004	2004–2005	2003–2005
Observations	16,791	16,505	14,639
F-statistic	11.76	12.02	11.80
Panel B: Different cut-off dates			
Tree cover	1.125	1.168	1.122
	(0.464)	(0.471)	(0.504)
Cut-off	2010–2014	2009–2015	2008–2017
Observations	22,006	19,462	14,692
F-statistic	14.67	13.68	12.57
Panel C: Sensitivity			
Tree cover	1.304	1.306	1.222
	(0.548)	(0.529)	(0.543)
Exposure	Buffer: 20m	Winsorizing: 90%	Winsorizing: 99%
Observations	15,830	15,884	15,884
F-statistic	15.28	15.39	11.87
Panel D: Additional controls			
Tree cover	1.014	1.089	1.106
	(0.395)	(0.420)	(0.456)
Controls	Amenities	Topography	Income
Observations	15,884	15,803	15,884
F-statistic	19.42	20.86	17.16
Panel E: Alternative specification			
Tree cover	1.058	1.060	1.133
	(0.444)	(0.436)	(0.481)
Weights	Postcode	Postcode/post	Postcode/year
Observations	199,665	199,665	199,665
F-statistic	18.83	17.51	12.12

Notes: Standard errors are reported between parentheses and are clustered at the ward level. All columns report the estimates from a long-difference IV specification in which the unit of observation is a postal code and the difference in tree cover is instrumented by the density of city-managed ash trees. The dependent variable is the difference in (log) transaction price. All specifications (except Panel E) include: ward fixed effects; a measure of city-managed tree density; latitude and longitude; area shares from the land classification in 2007 (tree canopy, grass/shrub, bare earth, water, buildings, roads, other paved surfaces and agriculture); and transaction controls in differences (except in Panel A, in which these characteristics are not available), including the number of rooms, the number of bedrooms, and 10 dwelling types (e.g., detached, apartment, duplex, commercial). In Panel A, the sample consists of observations between 2002 and 2006 (excluded from our baseline sample), and the dependent variable is constructed using pre-treatment and post-treatment periods as 2002–2003 and 2004–2006 (column 1), 2002–2004 and 2005–2006 (column 2), or 2002–2003 and 2005–2006 (column 3). In Panel B, we restrict the sample to 2007–2011/2014–2020 in column (1), 2007–2010/2015–2020 in column (2), 2007–2009/2016–2020 in column (3). In Panel C, we explore variations around the baseline specification: a buffer of 20m around postcodes in column (1), a winsorizing at 90% for publicly-managed densities in column (2), a winsorizing at 99% for publicly-managed tree densities in column (3). In Panel D, we condition the long-difference IV specification on: amenities (distance to green areas, ravines, schools, area share of sidewalk, length of pedestrian paths), topography (elevation, slope), and neighborhood income at baseline. In Panel E, the unit of observation is a transaction, the specification is regressing the (log) transaction price on the density of city-managed ash trees interacted with a post-treatment dummy, and the specifications include: (i) postcode fixed-effects; (ii) ward fixed effects interacted with year fixed effects; (iii) a measure of street tree density interacted with year fixed effects; (iv) latitude and longitude interacted with year fixed effects; (v) area shares from the land classification in 2007 (tree canopy, grass/shrub, bare earth, water, buildings, roads, other paved surfaces and agriculture) interacted with year fixed effects; and (vi) the number of rooms, the number of bedrooms, and 10 dwelling types interacted with year fixed effects.

C.2 Robustness checks

In this Appendix, we provide a systematic sensitivity analysis around the baseline specification reported in Panel A of Table 2.

Table C3 reports: placebo specifications (Panel A); specifications based on different cut-off dates for the pre- and post-treatment periods (Panel B); alternative buffers and winsorizing procedures to define tree densities (Panel C); robustness to extended controls for amenities, topography, or neighborhood income (Panel D); and an alternative specification at the transaction level (Panel E). First, one threat to identification is that the initial distribution of ash trees, partly reflecting urban developments in 1900–1930 and the associated distribution of elm trees, correlates with secular neighborhood dynamics. We reduce concerns about this identification threat by testing for the existence of pre-treatment differential trends. Specifically, we consider the period 2002–2006 in which we do observe property transactions, albeit with limited transaction controls, and estimate Equation (1) on this sample of transactions defining counterfactual pre-treatment and post-treatment periods as 2002–2003 and 2004–2006 (column 1), 2002–2004 and 2005–2006 (column 2), or 2002–2003 and 2005–2006 (column 3). It is reassuring that Panel A of Table C3 shows no differential trends before the treatment date. Second, Panel B considers transaction data from 2007 onward as in our baseline specification but defines alternative pre-treatment and post-treatment periods: 2007–2010 and 2014–2020 (column 1), 2007–2009 and 2015–2020 (column 2), or 2007–2008 and 2017–2020 (column 3). The estimates range between 1.12 and 1.17. Third, in Panel C, we consider minor alterations around our baseline specification: we construct land cover and ash tree density with a 20m buffer in column (1), instead of 10m; we winsorize non-zero values for ash tree density and all street tree density at 90% or 99%, rather than at 95% in the baseline. Again, the exercise confirms the robustness of our baseline estimations. Fourth, in Panel D, we condition our baseline specification on amenities (distance to green areas, ravines, schools, area share of sidewalk, length of pedestrian paths), on topography (elevation, slope), and on neighborhood income in 2011. Lastly, Panel E considers an alternative specification at the transaction level. Letting i denote a transaction with associated price P_{ipt} and L_p^t denote the inferred area share of tree canopy within the postcode p in the pre- (then coinciding with 2007) and post-treatment periods (then coinciding with 2018), we estimate:

$$\ln(P_{ipt}) = \alpha + \beta L_p^t + \gamma_t \mathbf{X}_{ipt} + \eta_p + \mu_t + \varepsilon_{ipt},$$

where L_p^t is instrumented by the density of publicly managed ash trees interacted with the post-EAB infestation dummy $Post_t$, $A_p \times Post_t$. In this specification, we include time-varying controls $\gamma_t \mathbf{X}_{ipt}$, capturing the evolution of the *time-varying* premium associated to: observable house characteristics (i.e., number of bedrooms, number of rooms, and type of dwelling); ward fixed effects; a measure of city-managed tree density; latitude and longitude; and area shares from the land classification in 2007 (tree canopy, grass/shrub, bare earth, water, buildings, roads, other paved surfaces and agriculture). The specifica-

tion thus flexibly controls for the differential evolution of prices across neighborhoods and time-varying returns to house characteristics. Standard errors are clustered at the ward level, as in our baseline specification. As in the baseline specification, we consider a sample of all transactions in 2007–2008 and in 2016–2020, and we define the post-period as 2016–2020. The only difference between columns (1), (2), and (3) is the definition of regression weights: in column (1), transactions are weighted such that each postal code contributes similarly to the estimates; in column (2), we weigh by the inverse number of observations in a postcode/time period; in column (3), we weigh by the inverse number of observations in a postcode/year. The results are identical to the long-difference specification.

Table C4. The value of trees—OLS estimates.

	House price	Temperature	Electricity	PM2.5 concentration
	(1)	(2)	(3)	(4)
Tree cover	-0.082	-1.517	-0.115	-0.006
	(0.041)	(0.173)	(0.027)	(0.004)
Observations	15,884	39,043	25,289	31,053

Notes: Standard errors are reported between parentheses and are clustered at the ward level. All columns report the estimates from a long-difference OLS specification in which the unit of observation is a postal code. All specifications include: ward fixed effects; a measure of city-managed tree density; latitude and longitude; and area shares from the land classification in 2007 (tree canopy, grass/shrub, bare earth, water, buildings, roads, other paved surfaces and agriculture). In column (1), the dependent variable is the difference in (log) transaction price, and we add transaction controls in differences, including the number of rooms, the number of bedrooms, and 10 dwelling types (e.g., detached, apartment, duplex, commercial). In column (2), the dependent variable is the difference in Land Surface Temperature (LST) computed as an average during July/August, and we control for the pre-treatment level of Land Surface Temperature within the postal code. In column (3), the dependent variable is the difference in (log) electricity consumption in July/August for the median household within a postal code and for all years between 2012–2020, and we control for the pre-treatment level of (log) electricity consumption within the postal code, as well as for gas expenditures. In column (4), the dependent variable is the difference in (log) concentration of PM2.5 in July/August (in $\mu g/m^3$), and we control for the pre-treatment level of PM2.5 concentration.

Table 2 (Panel A) provides estimates about the hedonic value of urban trees and their "ecosystem services". The TSLS specification reports the average treatment effect, leveraging the initial allocation of ash trees as exogenous variation in the dynamics of forest cover. In Table C4, we report the OLS estimates: we find that the correlations between changes in tree cover and changes in temperature (column 2) and energy consumption (column 3) are negative and significant, as in the TSLS specification, but three to four times smaller. One explanation could be measurement error in the inferred dynamics of urban forestry, which is better accounted for in the TSLS specification. The differences between the OLS and TSLS estimates for house prices and PM2.5 concentration are more substantial: the correlation between tree density and property values is negative and very small, in stark contrast with the TSLS estimates. One explanation could be that highly-demanded neighborhoods have a higher opportunity cost of maintaining urban forestry, biasing the OLS estimate downward. The same difference is observed for

PM2.5 concentration: OLS estimates could then be biased if land use, built-up density, or traffic (all affecting land surface temperature) were to evolve differently in more or less leafy neighborhoods.

Figure C2. Other tree species and the evolution of housing prices—a placebo check.

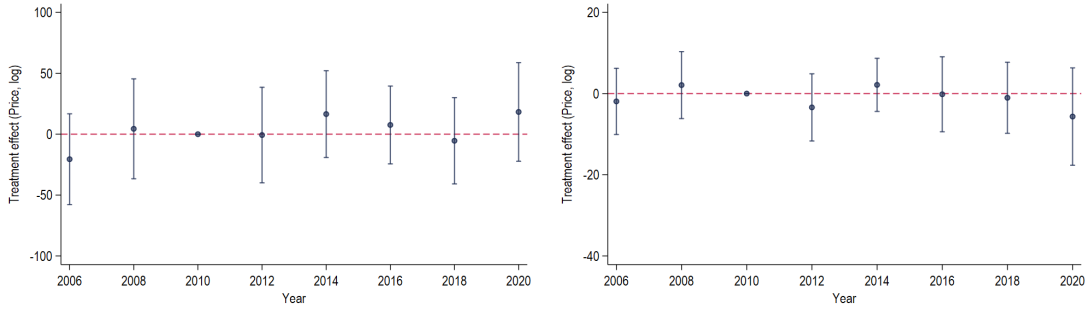

(a) Elm trees (b) Maple trees

Notes: This Figure shows the estimated correlation between elm/maple tree density and housing prices from 2006 (2007) to 2020. More specifically, we regress the (log) transaction price on a measure of elm/maple tree density (number of street elm/maple trees per area within a 10m buffer, as measured in 2010) interacted with period fixed effects, controlling for: (i) postcode fixed effects; (ii) ward fixed effects interacted with period fixed effects; (iii) a measure of city-managed tree density interacted with period fixed effects; (iv) latitude and longitude interacted with period fixed effects; and (v) area shares from the land classification in 2007 (tree canopy, grass/shrub, bare earth, water, buildings, roads, other paved surfaces and agriculture) interacted with period fixed effects. As in Figure 2 (b), a period groups two consecutive years for the sake of exposition. The reported coefficients are the ones in front of the measure of elm/maple tree density interacted with period fixed-effects, and vertical lines show 95 percent confidence intervals. Standard errors are clustered at the ward level, and the specification is weighted by the inverse of the number of observations in a given postcode.

Finally, we explore the possibility that diverging dynamics in housing demand and supply across neighborhoods with different levels of city-managed ash trees may drive our results. In a placebo specification building on the exercise of Figure 2 (b), we look at the time-varying relationship between home values and the distribution of other publicly-managed tree species (i.e., elm trees and maple trees). We replace the explaining variable by the density of publicly-managed elm trees or maple trees. While Figure 2 (b) was showing a gradual decrease in house prices in locations with a high density of publicly-managed ash trees at baseline, Figure C2 shows no such patterns for locations with a high density of publicly-managed elm trees or maple trees. This finding provides supporting evidence that the joint dynamics of urban forestry and property prices is indeed explained by the disappearance of *ash* trees.

D Tree canopy, temperature, energy consumption, and pollution

This section provides complements to the main estimation of ecosystem services provided by urban forestry.

Figure D1. The EAB infestation and the cooling effects of tree canopy over time.

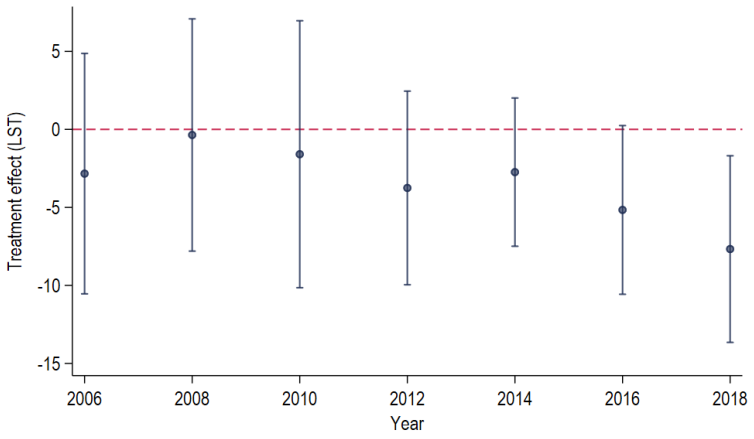

Notes: This Figure shows the estimated correlation between tree density and Land Surface Temperature (LST) for the months of July and August for each year between 2006 and 2018 (see Equation D1). More specifically, we regress the Land Surface Temperature (for a group of two consecutive years, τ) across postcodes on the measure of tree cover in 2018, instrumented by the number of street ash trees per area within a 10m buffer (as measured in 2010). We control for a measure of street tree density, ward fixed effects, latitude, longitude, and area shares for the land classification in 2007 (tree canopy, grass/shrub, bare earth, water, buildings, roads, other paved surfaces and agriculture). The reported coefficients are the ones in front of the measure of tree density, and vertical lines show 95 percent confidence intervals. Standard errors are clustered at the ward level

D.1 The cooling effect of urban forestry

We consider the following specification(s) to isolate the time-varying effects of the EAB infestation (through its impact on the tree canopy),

$$T_{pt} = \alpha + \beta_\tau L_p^{18} + \gamma \mathbf{X}_p + \varepsilon_p, \tag{D1}$$

where each observation is a postal code, T_{pt} is the average Land Surface Temperature within postcode p during July and August of a year t, and urban forestry in 2018, L_p^{18}, is instrumented by the density of ash trees at baseline, A_p. Controls include ward fixed effects, latitude and longitude, the density of publicly maintained trees, and area shares from the land classification in 2007. We estimate β_τ separately for each period of two consecutive years, τ, and report the estimates with their confidence intervals in Figure D1.

Intuitively, the estimates presented in Figure D1 are the causal effects of the catastrophe in each year, mitigated through the evolution of the tree canopy, i.e., the exercise can

be loosely interpreted as an event-study design. Figure D1 shows that the impact of the infestation starts to materialize after 2010. In 2018, a 10 percentage point additional tree cover within a postcode reduces temperature by about 0.8 degrees (Celsius). In theory, the gradient in the treatment effect could reflect two forces: (i) the tree felling is gradually implemented across the City of Toronto—as illustrated in Section 2—thus inducing higher treatment compliance over time; and (ii) there are secular trends in summer temperatures due to climate change.

D.2 Energy consumption

In this section, we highlight the time-varying effect of the EAB infestation on electricity consumption (during summer) between 2012–2020 in neighborhoods with high density of city-managed ash trees; we also provide a "placebo" test analyzing the relationship between urban forestry and electricity consumption during winter. Finally, we leverage episodes of high temperatures (resp. wind chill) to estimate the energy-consumption effect of urban forestry as a function of the solar-shading potential (resp. wind-sheltering potential) of the local urban forestry. Lastly, we provide details behind our back-of-the envelope calculations (see "Urban forestry and energy savings" in Section 4).

Figure D2. The EAB infestation and its energy consumption effects over time.

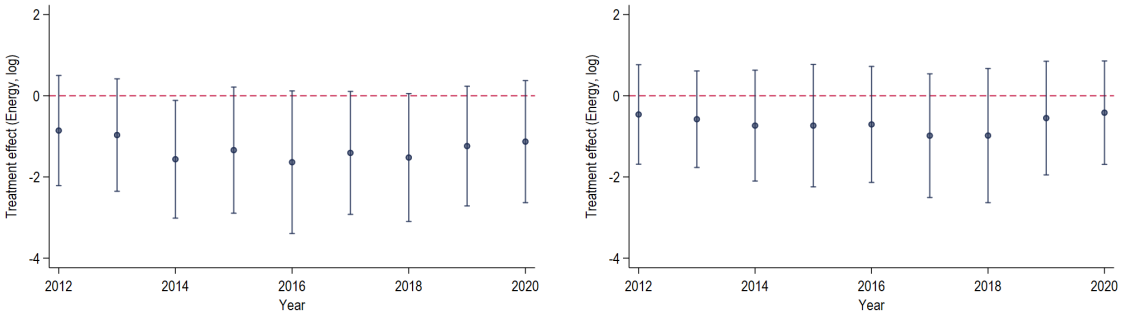

(a) July-August (2012–2020)

(b) December-February (2012–2020)

Notes: Panel (a) shows the estimated correlation between tree density and electricity consumption for the months of July and August for each year between 2012 and 2020 (in a specification similar to Equation D1). More specifically, we regress the (log) electricity consumption across postcodes on the measure of tree cover in 2018, instrumented by the number of street ash trees per area within a 10m buffer (as measured in 2010). We control for a measure of street tree density, ward fixed effects, latitude, longitude, and area shares for the land classification in 2007 (tree canopy, grass/shrub, bare earth, water, buildings, roads, other paved surfaces and agriculture). The reported coefficients are the ones in front of the measure of tree density, and vertical lines show 95 percent confidence intervals. Panel (b) replicates the exercise for winter months (December to February).

Energy consumption over time and across seasons We replicate the exercise of Figure D1 and Equation (D1) for average energy consumption across the summer months (July and August) in panel (a) of Figure D2. Note that, in contrast with Figure D1, we

do not observe electricity consumption before the start of the EAB infestation such that all years should be considered "treated", at least to some extent. We find a small gradient in energy consumption from 2012–2014 and a subsequent stabilization of the effect. In panel (b) of Figure D2, we look at electricity consumption as the dependent variable of Equation (D1), but we calculate it for the winter months (December to February). We consider this specification as a placebo test: the evolution of the tree canopy—as triggered by the EAB infestation—should matter most during summer. Panel (b) of Figure D2 indeed finds a more limited correlation between urban forestry and electricity saving during winter.

Figure D3. Shading effect of trees as a function of the time of the day and week.

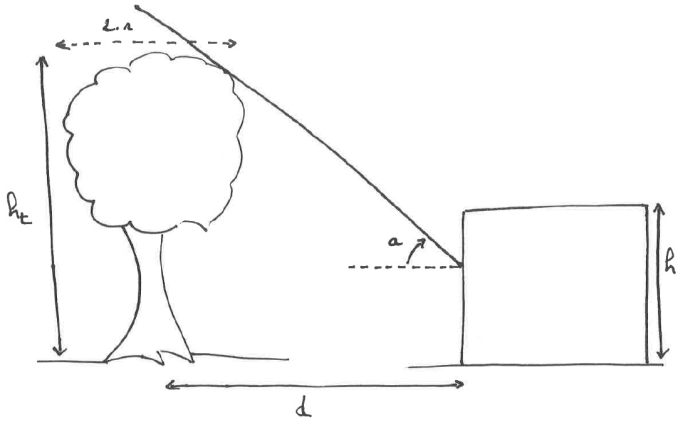

Notes: This Figure schematically represents the parameters used to derive the measure $Shade_{iw\tau}$, which depends on a week of the year w, a time of the day τ (a discrete interval of 15 minutes), and the surroundings of property i. We calculate the shade, $Shade_{iw\tau}$, as follows. At a given time of the day τ in week w, we identify the direction of the sun (in degrees, e.g., North would be 90 degrees) and the associated sun angle a. For instance, the sun angle would be generally lower during winter, and temporarily lower early in the day (when the direction is around 0 degrees) or late in the afternoon (when the direction is around 180 degrees). We then calculate the percentage of the house front covered in shade by the nearest tree (distance d) in the identified direction. This simplification allows us to ignore the trees behind this closest tree and to abstain from calibrating an imperfect shading provided by trees. For this exercise, we consider a house front to be between 2 and 7 meters, and we assume that trees are $h_t = 20$ meters high with a crown radius of $r = 5$ meters—both parameters being probably on the higher end of the tree size distribution. As apparent from the Figure, the percentage of the house front covered in shade is a simple function of the sun angle a, the height of the house, the distance to the tree, and the tree dimensions.

Construction of the shade and shelter measures In this section, we combine the relative positioning of trees and homes with solar angles and monthly wind roses across the year (as in Nikoofard et al., 2011; Upreti et al., 2017), in order to construct measures of *solar-shading potential* and *wind-sheltering potential*, which underlie our alternative empirical strategy based on the orientation of trees around homes. To facilitate the calculations of the solar-shading or wind-sheltering potential, we transform the "tree cover" surface into a discrete number of individual trees and we create a uniform grid of tree trunks every 10 meters inside the "tree coverage" surface. This procedure might induce

some measurement error, which would lead to an attenuation bias in assessing the impact of such measures on energy consumption.

For the shading potential of the neighboring tree canopy, we compute the measure S_{iw} for property i and week w of a given year as,

$$S_{iw} = \frac{\int Sun_{w\tau} \times Shade_{iw\tau} d\tau}{\int Sun_{w\tau} d\tau},$$

where τ is a time of the day (in practice, we divide the day into discrete intervals of 15 minutes), $Sun_{w\tau}$ is the potential sun exposure at time τ in week w , and $Shade_{iw\tau}$ is a measure of shade induced by the presence of trees around property i at time τ in week w. The variable $Shade_{iw\tau}$ is constructed by reconstituting the week-specific solar angle $a_w(\tau)$ and sun direction $\theta_w(\tau)$ as a function of time τ. At time τ, we select all trees in direction $\theta_w(\tau)$ originating from the centroid of a property. We then calculate the share of the property which is in the shade of these trees, $Shade_{iw\tau}$, exploiting the distance to the trees and the solar angle. This computation requires several assumptions regarding the height of a tree, the diameter of its crown, and the height of a property. We provide additional details about the computation in Figure D3. Note that we aggregate the property-specific measure, S_{iw}, into an average postcode measure, S_{pw}.

Figure D4. Sheltering effect of trees.

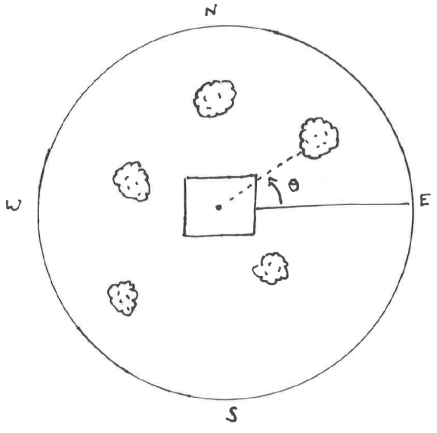

Notes: This Figure schematically represents the parameters used in order to derive the measure $Tree_{\theta i}$ used to construct the sheltering effect of trees. We combine the surroundings of property i with the direction of wind θ as follows: $Tree_{\theta i}$ is a dummy equal to 1 if there is a tree in direction θ and within 20 meters of the property.

To capture the sheltering potential of trees in the vicinity of property i in week w of a given year t, we compute,

$$W_{iwt} = \sum_{\theta=0}^{360} w_{\theta wt}(1 - Tree_{\theta i})p_{\theta wt},$$

where: $w_{\theta wt}$ is the Wind Chill Equivalent Temperature (WCET) used by Environment Canada, accounting for the average wind speed from direction θ (Celsius degrees); $Tree_{\theta i}$ is a dummy equal to 1 if there is a tree in direction θ and within 20 meters of the property; and $p_{\theta wt}$ is the probability that the wind originated from direction θ in week w of year t. We also compute a counterfactual measure for the Wind Chill Equivalent Temperature (WCET), ignoring the neighboring urban forestry:

$$W^c_{iwt} = \sum_{\theta} w_{\theta wt} p_{\theta wt}$$

In other words, any difference between W_{iwt} and W^c_{iwt} has to relate to the distribution of urban forestry. We illustrate the simple intuition behind the construction of measure W_{iwt} in Figure D4. We finally aggregate the property-specific measures, (W_{iwt}, W^c_{iwt}), into average postcode measures, (W_{pwt}, W^c_{pwt}).

Shade, shelter, and energy consumption To estimate the (local) cooling effect of urban forestry, we rely on a different empirical specification from that of the baseline strategy where we exploit short-run fluctuations in weather conditions at the weekly level. We run a simple difference-in-differences specification at the postcode level for all weeks w in year t between January 2011 and December 2015 (during which we have weekly energy consumption data, see Appendix Section B.3). Letting p denote a postcode, w a week and t a particular year, we estimate the following equation:

$$\ln(E_{pwt}) = \alpha + \beta_2 S_{pw} \times Temp_{wt} + \beta_1 S_{pw} + \beta_0 Temp_t + \delta_p + \nu_w + \mu_t + \varepsilon_{pwt}, \qquad \text{(D2)}$$

where E_{pwt} is a measure of energy consumption in a postcode/date, the measure S_{pw} captures the shade induced by surrounding trees in week w, thus depending on seasonal solar angles, and the measure $Temp_{wt}$ is a dummy equal to 1 during episodes of exceptionally high temperatures (within the top decile between May and September). The identification of the parameter β_2 reflects excess energy savings during extreme weather episodes in properties with higher *solar-shading potential*. The set of fixed effects ν_w and μ_t capture seasonality and trends in energy consumption; these fixed effects can also be interacted to clean for average consumption within a given week and isolate the (lower) excess consumption for properties surrounded by trees.

We run a similar regression during low-temperature episodes in order to estimate the wind-sheltering effect of urban forestry.[9] Letting p denote a postcode, w the week,

[9] Since 70 percent of energy used in the residential sector comes from oil or gas (Mohareb and Mohareb, 2014), we expect a stronger effect of wind-sheltering on gas consumption. However, some heating is electric and we still expect to find some effect.

and t the year, we estimate the following equation:

$$\ln(E_{pwt}) = a + b\,W_{pwt} + c\,W^{c}_{pwt} + \delta_p + \nu_w + \mu_t + \varepsilon_{pwt}, \tag{D3}$$

where the measures W_{pwt} and W^{c}_{pwt} are measures of wind chill—W_{pwt} accounting for the presence of surrounding trees and prevailing wind directions at that date. The identification of parameter b reflects excess energy savings during extreme (cold) weather episodes in properties with higher *wind-sheltering potential*. As before, ν_w and μ_t are week and year fixed effects that may also be interacted.

Figure D5. Excess energy consumption in extreme weather episodes and the relative positioning of trees.

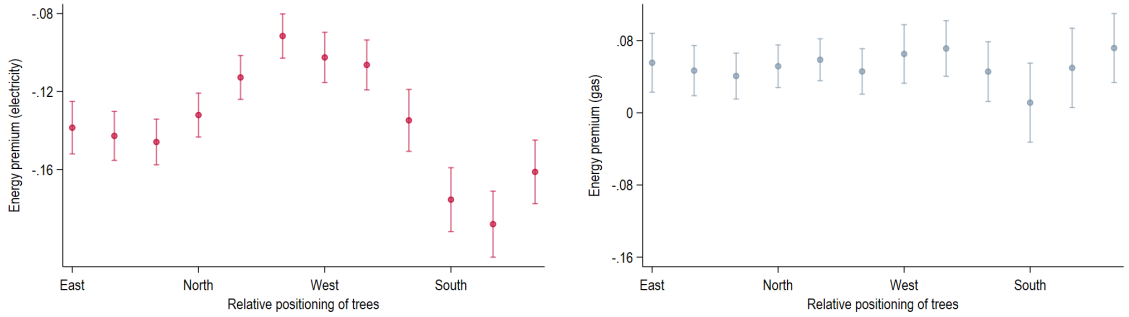

(a) Heat waves (b) Wind chill

Notes: This Figure represents the conditional correlations between energy consumption and the presence of trees in different directions from the average property within a postal code. Panel (a) reports the correlations between energy consumption and a dummy for heat waves interacted with the average number of trees within 10 meters for all houses of a given postal code in given directions (discretized between 0 and 360 degrees, with 30-degree intervals). Panel (b) reports the correlations between energy consumption and a dummy equal to 1 if the wind chill equivalent temperature is lower than 0 Celsius degrees during a given week interacted with the average number of trees in a certain direction across all houses of the postal code (East, North, West, South, every 30 degrees).

We now quantify the energy-saving effect of trees. For illustrative purposes, we will use figures to show our main findings, and we leave the underlying regression models to Tables D1 and D2. Panel (a) of Figure B10 describes the relationship between excess energy consumption during heat waves and the relative positioning of trees. We estimate the conditional correlation between excess energy consumption and surrounding trees as follows. We regress the postcode energy consumption on a dummy for heat waves, the average number of trees within 10 meters for all houses of a given postal code in a certain direction and their interaction, while controlling for time-fixed effects and postcode fixed-effects. Figure B10 reports the energy premium guaranteed by the presence of trees during heat waves (the interaction term), conditional on a given direction (discretized between 0 and 360 degrees, with 30-degree intervals). As apparent, the energy premium associated with the presence of a tree is not negligible. The premium is significant across all directions, but even more so in the East and South where shade

is likely to provide cooling. For instance, one additional tree for all houses of a given postal code—within 10 meters of each house and oriented South—is associated with a 18% decrease in energy consumption during heatwaves. One additional tree towards the North-West is associated with a 10% decrease in energy consumption.

Table D1. Energy consumption and the cooling effect of trees.

Energy consumption	(1)	(2)	(3)
Heat wave	0.1162	0.0522	0.0522
	(0.0141)	(0.0113)	(0.0113)
Heat wave × Shade	-0.1787	-0.1785	-0.1786
	(0.0243)	(0.0247)	(0.0247)
Observations	2,259,447	2,259,447	2,259,447
Fixed effects (postcode)	No	Yes	Yes
Fixed effects (time)	Year	Week/year	Week/year
Controls (historical temperature)	No	No	Yes

Standard errors are reported between parentheses and are clustered at the date-level. The unit of observation is a date × postcode.

Table D1 reports the estimates from Equation (D2). We find that heat waves increase energy consumption, but less so in neighborhoods with high average shading potential across houses. More specifically, consumption increases by about 12% in postal codes without trees and this premium reduces to $0.12 - 0.18 \times 0.26 \approx 7\%$ for neighborhoods within the highest percentile of shade potential (0.26).

Panel (b) of Figure B10 sheds light on the role of urban forestry during episodes of extreme cold. We regress the average energy consumption within a postal code on a dummy equal to 1 if the wind chill equivalent temperature is lower than 0 Celsius degrees during a given week, the average number of trees in a certain direction across all houses of the postal code (East, North, West, South, every 30 degrees), and their interaction, while controlling for time-fixed effects and postcode fixed-effects. The energy premium associated with the presence of a tree is not (significantly) different from 0: it is "higher" when winds originate from the South/East, possibly because such winds create a phenomenon called " lake-effect snow".[10]

Table D2 reports the estimates from Equation (D3). We find that a decrease of one degree (Celsius) during winter increases the weekly energy consumption by 0.36% for neighborhoods without urban forestry. The presence of a "blocking tree" in the path of the wind for all houses within the postal code reduces this effect to 0.22%. These

[10]Note that prevailing winds in Toronto blow from the West, sometimes from the South or North, but more rarely from the East.

Table D2. Energy consumption and the sheltering effect of trees.

Energy consumption	(1)	(2)	(3)
Wind chill (no shelter)	-0.0045	-0.0038	-0.0036
	(0.0005)	(0.0005)	(0.0005)
Wind chill (shelter)	0.0014	0.0014	0.0014
	(0.0003)	(0.0003)	(0.0003)
Observations	2,149,973	2,149,973	2,149,973
Fixed effects (postcode)	No	Yes	Yes
Fixed effects (time)	Year	Week/year	Week/year
Controls (historical temperature)	No	No	Yes

Standard errors are reported between parentheses and are clustered at the date-level. The unit of observation is a date × postcode. *Wind chill* is a measure of felt temperature accounting for wind speed (and shelter in the second row).

effects are markedly lower than the cooling effects of urban forestry during summer, as discussed in the next section.

D.3 The quantitative role of energy savings

This section complements the discussion about the quantification of energy savings.

Energy savings and the amenity value of urban forestry Table 2 shows that one percentage point in the area share of urban forestry reduces the average electricity consumption within a postal code by about 0.5%. This effect is however confined to four months (June-September); and the tree-saving effect is much lower during other times of the year. For instance, Figure D2 shows that the effect is about six-seven times lower during winter. Based on these causal estimates, we consider that one additional percentage point in tree cover reduces annual energy consumption by 0.17% through its cooling effect, and by 0.02% through its wind-sheltering properties—both effects being smoothed over a period of 12 months. Considering that the average monthly expenditure in our sample is around 200 Canadian Dollars (CAD) in 2018, those cumulative effects would amount to CAD 0.39 per month. In comparison, the associated increase in the flow value of a property of 1.13% would correspond to CAD 28 per month—a calculation based on the fact that the average monthly rent for a two-bedroom apartment was around CAD 2,500 in 2018.

Energy savings and maintenance costs The previous calculations are nested at the level of a household. In order to compare the energy benefits of urban forestry with its

maintenance costs, we need to aggregate those effects at the level of the City of Toronto. We also need to convert the cover in urban forestry into a number of trees.

First, please note that adding one tree within a postcode increases the area share of tree canopy by 0.45 percentage points (a calculation that we explain in Section 2); this 0.45 is the conversion rate that we will use thereafter. Second, from the previous calculations, adding a tree lowers the *annual* energy consumption by about CAD 2.1 *for each household* ($0.39 \times 12 \times 0.45$). With about 20 households per postcode, the total energy-saving benefit of a tree is thus CAD 42 per year.[11] Ignoring the opportunity costs of land usage, such energy benefits would be *much* larger than the maintenance costs of urban forestry (estimated at around CAD 4.20 in the 2011 City of Toronto Parks and Forestry budget proposal).

Figure D6. Electricity consumption and weekly temperature.

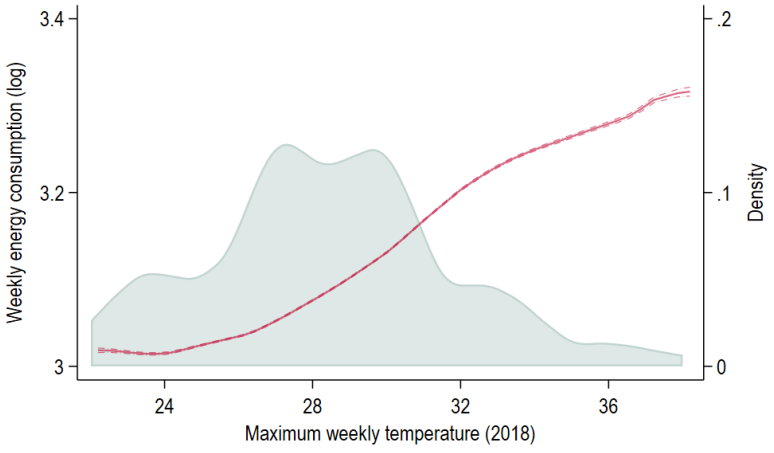

Notes: This Figure represents the relationship between the (weekly) energy consumption and the maximum weekly temperature. We group weeks by bins of weekly temperature: the dots represent the average energy consumption within each bin. The green area represents the distribution of the x-axis variable; and the sample is confined to summer months (July and August).

Energy savings in a changing climate With a non-linear relationship between temperature and energy consumption, there should be an increasing impact of urban forestry on energy savings over time—owing to the marked increase in the expected occurrence of heat waves.

We illustrate the non-linear relationship between temperature and energy consumption in Figure D6 where we leverage monthly data on electricity consumption between 2012 and 2020, which we match with maximum weekly temperature. We find that an

[11]The CAD 4-5 estimate cited in the main text refers to a 1-percentage-point increase in tree cover. Since a single tree increases canopy by only 0.45 percentage points, the corresponding per-tree energy savings is CAD 2.1 per household and year.

increase of temperature from 23 degrees (Celsius) to 24 degrees is not associated with any increase in electricity consumption. An increase of temperature from 27 degrees (Celsius) to 28 degrees increases electricity consumption by 3%; and an increase of temperature from 30 degrees (Celsius) to 32 degrees increases electricity consumption by 6%. The number of annual hours with average temperatures above 30 degrees (Celsius) is expected to double between 2020 and 2050, from an equivalent of 10 days to 20 days. According to these estimates, global warming would at most explain a doubling of the energy-saving premium by 2050.

D.4 Tree canopy and pollution

This section provides additional empirical analyses of the pollution-abatement effect of trees.

Figure D7. Pollution concentration over time.

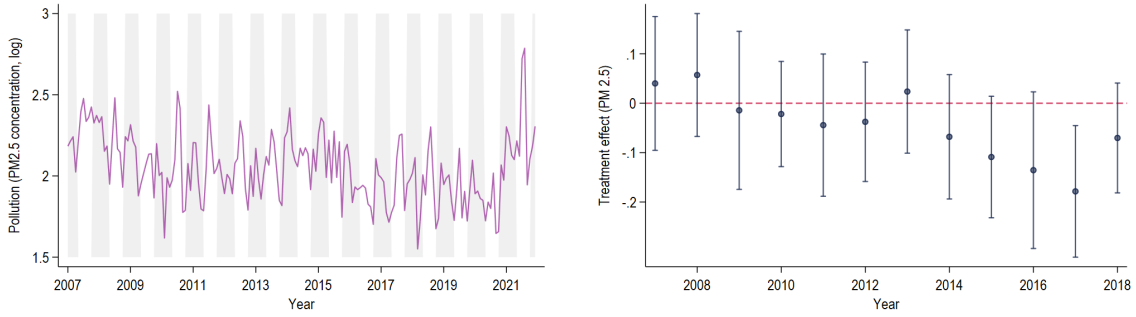

(a) Evolution over time

(b) Treatment effect

Notes: The left panel of the graph shows the monthly concentration of small particles (PM2.5, in $\mu g/m^3$) across postcodes in Toronto. The right panel shows the estimated correlation between tree density and (log) pollution for the months of July and August for each year between 2007 and 2018. More specifically, we regress (log) pollution across postcodes on the measure of tree cover in 2018, instrumented by the number of street ash trees per area within a 10m buffer (as measured in 2010). We control for a measure of street tree density, ward fixed effects, latitude, longitude, and area shares for the land classification in 2007 (tree canopy, grass/shrub, bare earth, water, buildings, roads, other paved surfaces and agriculture). The reported coefficients are the ones in front of the measure of tree density, and vertical lines show 95 percent confidence intervals.

Variation in pollution Panel (a) of Figure D7 illustrates seasonal and more secular variations in the concentration of fine particulate matter across the City of Toronto. The series is quite volatile and exhibits irregular seasonal patterns: pollution peaks are more frequent in summer, but a few occur in winter as well. There is no academic consensus about the local pollution-abatement effect of tree canopy (and its variation across seasons). Indeed, foliage prevents the dispersion of vehicle emissions (especially in road canyons, e.g., along the Don Valley Parkway), but increases the concentration of pollutants below the tree canopy (see, e.g., Salmond et al., 2013; Jin et al., 2014). We investigate

these effects within our context in the next section.

The pollution-abatement effect of trees We replicate the exercises discussed in Figures D1 and D2 (see Equation D1) to shed light on the dynamic impact of the EAB infestation. We report the year-specific estimates in Panel (b) of Figure D7; we see that the pollution-abatement effect of trees materializes between 2013 and 2016—the period in which city-managed ash trees were removed.

Table D3. The pollution-abatement effect of trees—a placebo and an aggregate specification.

Pollution (PM2.5)	(1)	(2)
Panel A: A placebo		
Tree cover	0.001	-0.005
	(0.001)	(0.008)
Observations	31,053	31,053
F-statistic	-	21.16
Panel B: An aggregate specification		
Tree cover	-0.086	-0.546
	(0.032)	(0.300)
Observations	379	379
F-statistic	-	0.16

Notes: Standard errors are clustered at the level of a ward and are reported between parentheses. In Panel A, the dependent variable is the difference in (log) concentration of PM2.5 in December/January (in $\mu g/m^3$), and we control for the pre-treatment level of PM2.5 concentration. In Panel B, the dependent variable is the difference in (log) concentration of PM2.5 in July/August (in $\mu g/m^3$), and we control for the pre-treatment level of PM2.5 concentration, but all observations are nested at a more aggregate level than a postal code, i.e., a neighborhood characterized by the first 4 characters of a postal code. Across both panels, column (1) reports the OLS estimate while column (2) reports the estimates from a long-difference IV specification where the difference in tree cover is instrumented by a measure of ash tree density. All specifications include: latitude and longitude; the density of publicly maintained trees; and area shares from the land classification in 2007.

The pollution-abatement effect of trees We conduct a placebo exercise in Panel A of Table D3, in which we replicate column (4) of Table 2 (and column 4 of Table C4) with PM2.5 concentration *during winter* (December, January) as the dependent variable. Both the OLS and the IV specifications provide negligible estimates. The absence of foliage indeed limits the impact of a tree canopy, whether positive or negative (Salmond et al., 2013; Jin et al., 2014).

In Panel B of Table D3, we replicate column (4) of Table 2 (and column 4 of Table C4) but nested at the level of a "neighborhood", characterized by the first 4 characters of a postal code. This specification—based on more aggregate spatial units to replicate the spatial auto-correlation in the measurement of PM2.5 concentration—delivers a negative

effect of urban forestry on pollutant concentration, but the TSLS specification is then under-powered because administrative divisions above the postal codes are relatively large.

Benchmarking the pollution estimates against the literature Our main pollution estimates are comparable to those reported in Venter et al. (2024), who utilize similar data. These authors highlight the variability and context specificity of green spaces' impact on urban air pollution levels. Trees moderate air pollution primarily through deposition, where air pollutants are absorbed by vegetation, and dispersion, which dilutes concentrations of air pollutants. While exploring these mechanisms in detail falls outside the scope of our paper, it is important to acknowledge that dispersion effects may account for the relatively modest reduction in pollution levels.

References

Abadie, Alberto, "Using Synthetic Controls: Feasibility, Data Requirements, and Methodological Aspects," *Journal of Economic Literature*, June 2021, *59* (2), 391–425.

Abatzoglou, John, Solomon Dobrowski, Sean Parks, and Katherine Hegewisch, "TerraClimate, a high-resolution global dataset of monthly climate and climatic water balance from 1958–2015," *Scientific Data*, 2018, *5* (1), 1–12.

Arkhangelsky, Dmitry, Susan Athey, David A Hirshberg, Guido W Imbens, and Stefan Wager, "Synthetic difference-in-differences," *American Economic Review*, 2021, *111* (12), 4088–4118.

Aukema, Juliann, Brian Leung, Kent Kovacs, Corey Chivers, Kerry Britton, Jeffrey Englin, Susan Frankel, Robert Haight, Thomas Holmes, Andrew Liebhold, Deborah McCullough, and Betsy Von Holle, "Economic impact of non-native forest pests in the continental United States," *PLoS One*, 2011, *6* (9).

Benson, Earl D, Julia L Hansen, Arthur L Schwartz, and Greg T Smersh, "Pricing residential amenities: the value of a view," *The Journal of Real Estate Finance and Economics*, 1998, *16* (1), 55–73.

Brown, Christopher, Steven Brumby, Brookie Guzder-Williams, Tanya Birch, Samantha Brooks Hyde, Joseph Mazzariello, Wanda Czerwinski, Valerie Pasquarella, Robert Haertel, Simon Ilyushchenko et al., "Dynamic World, Near real-time global 10m land use and land cover mapping," *Scientific Data*, 2022, *9* (1), 251.

City of Toronto, "2018 Tree Canopy Study," Technical Report, Report from the General Manager, Parks, Forestry and Recreation 2019.

Donkelaar, Aaron Van, Melanie Hammer, Liam Bindle, Michael Brauer, Jeffery Brook, Michael Garay, Christina Hsu, Olga Kalashnikova, Ralph Kahn, Colin

Lee et al., "Monthly global estimates of fine particulate matter and their uncertainty," *Environmental Science & Technology*, 2021, *55* (22), 15287–15300.

Eichholtz, Piet, Nils Kok, and John M. Quigley, "Doing well by doing good? Green office buildings," *American Economic Review*, 2010, *100* (5), 2492–2509.

Ermida, Sofia, Patrícia Soares, Vasco Mantas, Frank-M. Göttsche, and Isabel Trigoe, "Google Earth Engine open-source code for Land Surface Temperature estimation from the Landsat series," *Remote Sensing*, 2020, *12*, 1471.

Han, Lu, Stephan Heblich, Christopher Timmins, and Yanos Zylberberg, "Replication data for: "Cool cities: The value of urban trees"," *American Economic Review: Insights [publisher]; Inter-University Consortium for Political and Social Research, Ann Arbor, MI. [distributor]*, 2025, *https://doi.org/10.3886/E240953V1.*

Hengl, Tomislav, "Soil bulk density (fine earth) 10 x kg / m-cubic at 6 standard depths (0, 10, 30, 60, 100 and 200cm) at 250m resolution," 2018.

_ **and Ichsani Wheeler**, "Soil organic carbon content in x 5 g / kg at 6 standard depths (0, 10, 30, 60, 100 and 200cm) at 250m resolution," 2018.

Herms, Daniel and Deborah McCullough, "Emerald ash borer invasion of North America: history, biology, ecology, impacts, and management," *Annual Review of Entomology*, 2014, *59*, 13–30.

Hijmans, Robert, Susan Cameron, Juan Parra, Peter Jones, and Andy Jarvis, "Very high resolution interpolated climate surfaces for global land areas," *International Journal of Climatology: A Journal of the Royal Meteorological Society*, 2005, *25* (15), 1965–1978.

Jarvis, Andy, Hannes Isaak Reuter, Andrew Nelson, Edward Guevara et al., "Hole-filled SRTM for the globe Version 4," *available from the CGIAR-CSI SRTM 90m Database*, 2008, *15* (25-54), 5.

Jin, Sijia, Jiankang Guo, Stephen Wheeler, Liyan Kan, and Shengquan Che, "Evaluation of impacts of trees on PM2.5 dispersion in urban streets," *Atmospheric Environment*, 2014, *99*, 277–287.

Li, Zhao-Liang, Hua Wu, Si-Bo Duan, Wei Zhao, Huazhong Ren, Xiangyang Liu, Pei Leng, Ronglin Tang, Xin Ye, Jinshun Zhu et al., "Satellite remote sensing of global land surface temperature: Definition, methods, products, and applications," *Reviews of Geophysics*, 2023, *61* (1), e2022RG000777.

Manoli, Gabriele, Simone Fatichi, Markus Schläpfer, Kailiang Yu, Thomas W Crowther, Naika Meili, Paolo Burlando, Gabriel G Katul, and Elie Bou-Zeid, "Magnitude of urban heat islands largely explained by climate and population," *Nature*, 2019, *573* (7772), 55–60.

Mohareb, Eugene A. and Adrian K. Mohareb, "A comparison of greenhouse gas emissions in the residential sector of major Canadian cities," *Canadian Journal of Civil Engineering*, 2014, *41* (4), 285–293.

Naserikia, Marzie, Melissa A Hart, Negin Nazarian, Benjamin Bechtel, Mathew Lipson, and Kerry Nice, "Land surface and air temperature dynamics: The role of urban form and seasonality," *Science of The Total Environment*, 2023, *905*, 167306.

Nikoofard, Sara, V. Ismet Ugursal, and Ian Beausoleil-Morrison, "Effect of external shading on household energy requirement for heating and cooling in Canada," *Energy and Buildings*, 2011, *43* (7), 1627 – 1635.

Nowak, David and Eric Greenfield, "Declining urban and community tree cover in the United States," *Urban Forestry & Urban Greening*, 2018, *32*, 32–55.

Peng, Shushi, Shilong Piao, Philippe Ciais, Pierre Friedlingstein, Catherine Ottle, François-Marie Bréon, Huijuan Nan, Liming Zhou, and Ranga Myneni, "Surface urban heat island across 419 global big cities," *Environmental Science & Technology*, 2012, *46* (2), 696–703.

Price, Colin, "Quantifying the aesthetic benefits of urban forestry," *Urban Forestry & Urban Greening*, 2003, *1* (3), 123–133.

Sadof, Clifford S, Deborah G McCullough, and Matthew D Ginzel, "Urban ash management and emerald ash borer (Coleoptera: Buprestidae): facts, myths, and an operational synthesis," *Journal of Integrated Pest Management*, 08 2023, *14* (1), 14.

Salmond, J.A., D.E. Williams, G. Laing, S. Kingham, K. Dirks, I. Longley, and G.S. Henshaw, "The influence of vegetation on the horizontal and vertical distribution of pollutants in a street canyon," *Science of the Total Environment*, 2013, *443*, 287–298.

Sanderson, Eleanor and Frank Windmeijer, "A weak instrument F-test in linear IV models with multiple endogenous variables," *Journal of econometrics*, 2016, *190* (2), 212–221.

Theobald, David, Dylan Harrison-Atlas, William Monahan, and Christine Albano, "Ecologically-relevant maps of landforms and physiographic diversity for climate adaptation planning," *PloS One*, 2015, *10* (12), e0143619.

Todorova, Assenna, Shoichiro Asakawa, and Tetsuya Aikoh, "Preferences for and attitudes towards street flowers and trees in Sapporo, Japan," *Landscape and Urban Planning*, 2004, *69* (4), 403–416.

Upreti, Ruby, Zhi-Hua Wang, and Jiachuan Yang, "Radiative shading effect of urban trees on cooling the regional built environment," *Urban Forestry and Urban Greening*, 2017, *26*, 18–24.

Venter, Zander S., Amirhossein Hassani, Erik Stange, Philipp Schneider, and Nuria Castell, "Reassessing the role of urban green space in air pollution control," *Proceedings of the National Academy of Sciences*, 2 2024, *121.*

Zanaga, Daniele, Ruben Van De Kerchove, Dirk Daems, Wanda De Keersmaecker, Carsten Brockmann, Grit Kirches, Jan Wevers, Oliver Cartus, Maurizio Santoro, Steffen Fritz et al., "ESA WorldCover 10 m 2021 v200," 2022.